

Fragment-based discovery of a new class of inhibitors targeting mycobacterial tRNA modification

Sherine E. Thomas^{*1}, Andrew J. Whitehouse^{*2}, Karen Brown^{3,4}, Juan M. Belardinelli⁵, Ramanuj Lahiri⁶, M. Daben J. Libardo⁷, Pooja Gupta¹, Sony Malhotra⁸, Helena I. M. Boshoff⁷, Mary Jackson⁵, Chris Abell², Anthony G. Coyne², Tom L. Blundell^{§1}, R. Andres Floto^{3,4}, Vítor Mendes^{§1}

¹ Department of Biochemistry, University of Cambridge, 80 Tennis Court Road, Cambridge, CB2 1GA, UK

² Department of Chemistry, University of Cambridge, Lensfield Road, Cambridge, CB2 1EW, UK.

³ MRC Laboratory of Molecular Biology, Francis Crick Avenue, Cambridge, CB2 0QH, UK.

⁴ Cambridge Centre for Lung Infection, Royal Papworth Hospital, Cambridge, CB23 3RE, UK.

⁵ Mycobacteria Research Laboratories, Department of Microbiology, Immunology and Pathology, Colorado State University, Fort Collins, Colorado, USA.

⁶ National Hansen's Disease Program, Healthcare Systems Bureau, HRSA, DHHS, USA.

⁷ Tuberculosis Research Section, Laboratory of Clinical Immunology and Microbiology, National Institute of Allergy and Infectious Disease, National Institutes of Health, 9000 Rockville Pike, Bethesda, Maryland 20892, USA.

⁸ Birkbeck College, University of London, Malet Street, WC1E7HX, UK

* Contributed equally

§ To whom correspondence should be addressed

Key words: Structure-guided; Fragment-based; Mycobacteriaceae; *Mycobacterium abscessus*; *Mycobacterium tuberculosis*; Cystic Fibrosis; TrmD.

Abbreviations: DSF – differential scanning fluorimetry; FBDD – fragment-based drug discovery; LE – ligand efficiency; MIC – minimum inhibitory concentration; NTM – nontuberculous mycobacteria; SAH – *S*-adenosyl-L-homocysteine; SAM – *S*-adenosyl-L-methionine.

1 **Abstract**

2 Translational frameshift errors are often deleterious to the synthesis of functional proteins as
3 they lead to the production of truncated or inactive proteins. TrmD (tRNA-(N(1)G37)
4 methyltransferase) is an essential tRNA modification enzyme in bacteria that prevents +1 errors
5 in the reading frame during protein translation and has been identified as a therapeutic target
6 for several bacterial infections. Here we validate TrmD as a target in *Mycobacterium abscessus*
7 and describe the application of a structure-guided fragment-based drug discovery approach for
8 the design of a new class of inhibitors against this enzyme. A fragment library screening
9 followed by structure-guided chemical elaboration of hits led to the development of compounds
10 with potent *in vitro* TrmD inhibitory activity. Several of these compounds exhibit activity
11 against planktonic *M. abscessus* and *Mycobacterium tuberculosis*. The compounds were further
12 active in macrophage infection models against *Mycobacterium leprae* and *M. abscessus*
13 suggesting the potential for novel broad-spectrum mycobacterial drugs.

14

15

16

17

18

19

20

21

22

23

24

25

26 Introduction

27 Mycobacteria are a group of diverse organisms that include many important human pathogens.
28 Within this group, *Mycobacterium tuberculosis*, the causative agent of tuberculosis, is
29 responsible for over 1.7 million deaths per year (Floyd et al., 2018). Nevertheless,
30 *Mycobacterium abscessus*, a rapidly growing species of nontuberculous mycobacteria (NTM),
31 has recently emerged as a major threat to individuals with Cystic Fibrosis (CF) and other
32 chronic inflammatory lung conditions (Bar-On et al., 2015; Sood and Parrish, 2017), with
33 infection rates increasing around the world (Floto et al., 2016). *M. abscessus* is intrinsically
34 resistant to most antibiotics and is consequently associated with extremely high treatment
35 failure rates (Floto et al., 2016). There is therefore an urgent unmet need to develop new
36 antibiotics.

37 Several structurally diverse, modified nucleosides, found at different locations of tRNAs, help
38 in the maintenance of the reading frame and avoidance of translational frame-shift errors. Many
39 such nucleoside modifications are found in regions near the anticodon, particularly at position
40 34 (the wobble position) and 37 (3' and adjacent to the anticodon) of tRNA (Ahn et al., 2003;
41 Urbonavicius et al., 2001). TrmD, tRNA-(N(1)G37) methyltransferase, catalyzes the
42 methylation of G₃₇ (Guanosine at position 37) in prokaryotic tRNAs (**Figure 1A**). This
43 modified nucleotide N¹-methylguanosine at position 37 (m¹G₃₇) is present in tRNAs containing
44 a G₃₆G₃₇ sequence in the anti-codon region from all three domains of life, where G₃₇ is the base
45 adjacent to the anticodon at the 3' end (Ahn et al., 2003; Bjork et al., 2001; Bjork et al., 1989).
46 Mutations in *trmD* result in growth defects associated with increased translational
47 frameshifting leading to defective protein production (Bjork et al, 1989; Urbonavicius, 2001).
48 TrmD belongs to a distinct class of *S*-adenosyl-L-methionine (SAM)-dependent
49 methyltransferases known as the SpoU-TrmD (SPOUT) RNA methyltransferase superfamily

50 or Class IV methyltransferases. Proteins belonging to this family are structurally unique due to
51 the absence of a consensus methyltransferase fold. TrmD and other proteins of the SPOUT
52 family consist of a deep trefoil knot architecture at the catalytic region, which provides an L-
53 shaped pocket for binding of SAM. In eukaryotes however, G₃₇ methylation is carried out by
54 the enzyme Trm5, belonging to the Class I methyltransferase family (Anantharaman et al.,
55 2002; Hori, 2017; Ito et al., 2015).

56 Previous research (Goto-Ito et al., 2009; Ito et al., 2015) has shown that TrmD and Trm5 have
57 distinct substrate requirements with RNA. While Trm5 recognizes the overall L-shaped tertiary
58 structure of tRNA possessing a G₃₇ base, TrmD recognition involves mainly the D stem and
59 anticodon stem loop of tRNA with G₃₆G₃₇ bases. Trm5 functions as a monomer and binds to
60 SAM at the Rossmann fold region of the active site, in contrast to dimeric TrmD with a trefoil
61 knot methyl donor binding region. Further, SAM adopts a unique bent conformation in TrmD
62 as compared to the extended conformation in Trm5 and many other canonical
63 methyltransferases. These distinct structural features, substrate requirements and ligand
64 binding conformations provide the potential for designing novel and selective inhibitors of
65 bacterial TrmD (Goto-Ito et al., 2017).

66 A previous drug discovery effort targeting *Haemophilus influenzae* TrmD (Hill et al., 2013)
67 led to the development of selective inhibitors with potent biochemical activity against TrmD
68 isozymes *in vitro*. However, these compounds in general only showed weak antibacterial
69 activity when profiled against a range of Gram-positive and Gram-negative pathogens,
70 including against recombinant strains of *E. coli* and *H. influenzae* debilitated in the AcrAB
71 TolC efflux pumps (Hill et al., 2013). A recent drug discovery work was reported against
72 *Pseudomonas aeruginosa* TrmD which reported potent inhibitors of this enzyme. However,
73 the antibacterial activity of these was weak not only against *P. aeruginosa* but also against
74 other bacteria including mycobacteria (Zhong et al., 2019).

75 Fragment-based drug discovery (FBDD) is a promising approach for the identification of new
76 drugs, whereby the complexity of the chemicals screened is reduced by decreasing their
77 molecular weights (typically < 300 Da), which at the same time increases their promiscuity in
78 binding targets. Initial fragment hits usually exhibit lower potency than the more complex drug-
79 like molecules found in typical high-throughput screening compound libraries. However, such
80 fragments bind by making well-defined and directional interactions, giving rise to highly ligand
81 efficient (LE) molecules. These fragments can then be chemically optimized into lead
82 candidates, thereby more effectively exploring the chemical space available for binding to the
83 target protein (Erlanson et al., 2016; Mendes and Blundell, 2016; Murray et al., 2014; Thomas
84 et al., 2017). In this work we validate TrmD as a mycobacterial target and describe the
85 application of an FBDD approach to generate a new family of small-molecule inhibitors of *M.*
86 *abscessus* TrmD, having anti-microbial activities against a range of pathogenic mycobacteria.

87

88 **Results**

89 **TrmD is essential for *M. abscessus***

90 Previous studies have demonstrated that *trmD* is essential in diverse bacteria including *M.*
91 *tuberculosis*, where different transposon mutagenesis studies have shown that it is essential or
92 that mutants had a growth defect (DeJesus et al., 2017; Griffin et al., 2011; Sasseti et al., 2003).
93 However, confirmation of essentiality of *trmD* for *M. abscessus* was lacking. Three initial
94 attempts to disrupt the *trmD* gene of *M. abscessus* subsp. *massiliense* CIP108297 by
95 homologous recombination using a recombineering approach proved unsuccessful. To
96 determine whether the *trmD* gene is required for *M. abscessus* growth, allelic replacement
97 experiments were repeated in the background of a *M. abscessus* subsp. *massiliense* CIP108297
98 merodiploid expressing a second copy of the *trmD* gene from the integrative plasmid
99 pMV306H::*trmD*, and in a control *M. abscessus* subsp. *massiliense* CIP108297 strain

100 harbouring an empty pMV306H plasmid. Analysis of over 100 candidate mutants in each
101 background from two independent experiments showed that the endogenous chromosomal
102 copy of *trmD* could be knocked-out in the presence of an extra-copy of the gene but not in *M.*
103 *abscessus* cells carrying an empty plasmid (**Figure 1B**), thus confirming *trmD* essentiality for
104 *M. abscessus* growth.

105

106 ***M. abscessus* TrmD: overall structure and ligand binding**

107 We determined the crystal structures of *M. abscessus* TrmD in apo form at 1.60 Å resolution
108 (PDB code **6NVR**), as well as in complex with SAM and *S*-adenosyl-L-homocysteine (SAH)
109 at 1.67 Å and 1.48 Å resolution respectively (PDB codes **6NW6** & **6NW7**). The crystals belong
110 to space group P2₁2₁2₁ and consist of a homodimer in the asymmetric unit. Each non-
111 crystallographic two-fold symmetry-related protomer of TrmD interacts in an antiparallel
112 manner and consists of two domains: a larger *N*-terminal domain spanning residues 1-161 and
113 a smaller *C*-terminal helical domain (177-242) connected by a flexible inter-domain linker.
114 The two domains of the individual protomers do not contact each other and the inter-domain
115 region is largely disordered, with residues 162-177 not clearly visible in the apo structure
116 (**Figure 1 C & D**).

117 The SAM binding region of TrmD is located at the base of the *N*-terminal domain and consists
118 of a deep trefoil knot architecture, made of three distinct untwisted loop regions. The trefoil
119 knot of *M. abscessus* TrmD is made up of a cover loop spanning residues ⁸⁴TPAG⁸⁷ between
120 strand β₃ and helix α₄ leading to the wall loop at the edge of the methionine pocket containing
121 residues ¹⁰⁹GRYEGID¹¹⁵ between β₄ and helix α₅. This loop then crosses over to form the
122 bottom loop with residues 132-140 that encompasses the SAM adenine ring between strand β₅
123 and helix α₆ (**Figure 2 A & B**). SAM and SAH occupy the deep trefoil-knot active site at the
124 base of the *N*-terminal region and adopt an L-shaped bent conformation as previously observed

125 with other TrmD orthologs (Christian et al., 2016; Koh et al., 2017). Both SAM and SAH form
126 an extensive hydrogen-bonding network in this region along with hydrophobic and π -
127 interactions as shown in **Figure 2 B & C**. The adenine ring of SAM and SAH is sandwiched
128 between the cover loop and bottom loop of the knot with the adenine N1 and N7 forming
129 hydrogen-bond contacts with the backbone amide-nitrogen atoms of Ile133 and Leu138
130 respectively, while the amino nitrogen forms additional hydrogen bonding contacts with the
131 backbone carbonyl oxygen atoms of Gly134 and Tyr136 of the bottom loop (**Figure 2 B &**
132 **S2**).

133 The ribose and methionine moieties of SAM and SAH interact with the wall and bottom loops
134 of the knot. The hydroxyl oxygen atom (O2') of the ribose ring forms a hydrogen bond with
135 the backbone amide of Gly109. The methionine and homocysteine moieties further extend into
136 the active site groove formed between the cover and wall loops, making further hydrogen-
137 bonding interactions with water molecules in this region (**Figure 2 B & S2**).

138 A structural superposition of the apo and SAM bound forms of TrmD reveals the wall loop
139 undergoing a switch in conformation leading to a movement of about 5 Å, when measured at
140 the C α of Tyr111, to the outer edge of subunit A. This conformational flip of the wall loop
141 from apo form to SAM-bound form and the subsequent change in positions of residues 110 to
142 113 help to accommodate the methionine moiety of the methyl donor (**Figure 2 A & B**).

143

144 **Fragment Screening, hit validation and clustering of fragments**

145 Having examined the conformational changes and binding interactions at the *M. abscessus*
146 TrmD catalytic site, we initiated a structure-guided FBDD effort targeting *M. abscessus* TrmD
147 by screening an in-house library of 960 small molecule fragments. The preliminary screening
148 was performed using differential scanning fluorimetry (DSF), resulting in 53 hits within a
149 thermal shift cut-off value of 3 standard deviations from the negative control, consisting of

150 TrmD protein in the absence of any ligand. These hits were then selected for validation by X-
151 ray crystallography. Apo crystals of *M. abscessus* TrmD were soaked with each of the 53
152 fragments in individual experiments. The resulting crystal structure determinations allowed
153 characterization of the binding modes of 27 fragments (**Figure S3**).

154 All of the 27 fragments, validated by X-ray crystallography, were found to occupy the TrmD
155 SAM site. These fragments can be clustered into three groups based on their binding mode at
156 this site (**Figure 2 D & S3**). **Cluster 1** consists of 12 fragments that bind exclusively to the
157 sub-pocket that accommodates the adenine ring of SAM, engaging residues within the cover
158 and bottom loops of the trefoil knot. These fragments recapitulated many of the hydrogen
159 bonding and π -interactions of the SAM adenine moiety, as shown in the example (**Figure 2 D**
160 **& S3**). These interactions include hydrogen-bond contacts to the side chain of Ser132, which
161 in turn adopts a dual conformation, and to the backbone amides of Ile133, Gly134, Tyr136 and
162 Leu138.

163 The **second cluster** consists of 12 further fragments that occupy the entire adenosine region of
164 the TrmD active site, thus extending from adenine towards the ribose-binding pocket of the
165 active site. These fragments, in addition to retaining several adenine moiety contacts, also
166 interact with the wall loop residues, forming hydrogen bonds to the backbone amides of Tyr111
167 and Gly109 and water-mediated hydrogen bonds as shown in the example (**Figure 2 D & S3**).

168 **Cluster 3** consists of three fragments that extend beyond the TrmD adenosine site, thus
169 reaching the methionine-binding region of the pocket. One of these fragments, fragment **8**
170 stretched further into the groove formed between the cover and wall loops of the trefoil knot,
171 thus engaging additional hydrogen bonding contacts with the side chain of Thr84 and the back
172 bone amide of Gly109 in this region (**Figure 2 D & S3**).

173

174

175 **Fragment merging & hotspot mapping for chemical elaboration**

176 Two of the above 27 fragment hits, fragments **23** (K_d 0.17 mM, LE 0.37) and **24** (K_d 0.26 mM,
177 LE 0.41), were chosen for further chemical development by a fragment-merging strategy. The
178 choice of fragments for subsequent chemical optimization was based on a number of criteria,
179 including binding affinity, ligand efficiency, synthetic tractability and their ability to make key
180 binding interactions at the TrmD SAM binding site. Fragment **23** occupies the adenosine
181 binding region of the TrmD AdoMet site, with its pyrazole ring making hydrogen bond contacts
182 to the backbone amides of Tyr136 and Leu138 and the amino group making further hydrogen
183 bonds with the backbone carbonyl oxygen of Gly134 and the side chain of Ser132, respectively.
184 The 4-methoxyphenyl ring of the fragment extends into the ribose binding site, engaging
185 hydrophobic and π -interactions with the residues of the cover loop (**Figure 3A & S3**).

186 The indole ring of fragment **24** also occupies the ribose pocket where it forms a water-mediated
187 interaction with the backbone amide nitrogen of Leu138. The 4-methoxyphenyl and indole ring
188 systems of fragments **23** and **24** overlap perfectly, while the 6-boronic acid group of fragment
189 **24** partially extends into the SAM adenine pocket and makes hydrogen bonds with the
190 backbone amides of residues Tyr136 and Leu138 and further water-mediated hydrogen bond
191 contacts to the backbone amides of Val131, Ile133, Gly134 and the side chain hydroxyl group
192 of Ser132 (**Figure 3A & S3**). Compound **AW1** (K_d 0.11 mM, LE 0.36, IC_{50} 0.23 mM), formed
193 by merging the two fragments, adopts a similar conformation to that of the original fragments
194 in the TrmD SAM site, as shown in **Figures 3 B & C**, thereby providing a new chemical
195 scaffold for further structure-guided development.

196 To aid the structure-guided lead discovery, the binding propensities of TrmD protein to ligands
197 were further examined using the hotspot-mapping program developed by Radoux and co-
198 workers (Radoux et al., 2016) . Hotspots are areas within the protein that provide relatively
199 large contributions to the overall binding affinity of ligands (Hajduk et al., 2005; Ichihara et al.,

200 2014). This is usually mediated by the displacement of water molecules having restricted
201 freedom owing to their location within a hydrophobic cavity or close to a patchwork of
202 hydrogen bonds and lipophilic amino acid side chains, thus compensating for the loss of entropy
203 on binding. These regions not only satisfy the minimum binding requirement for fragments but
204 also maintain the original fragment binding interactions when elaborated (Radoux et al., 2016).
205 While the observed fragment hits and the corresponding merged compound **AW1** satisfy many
206 of the predicted protein-hotspot interactions, the map suggests further interactions that stabilise
207 elaborated fragments, sometimes allowing them to reach other hotspots that are not yet
208 explored. As shown in the example (**Figure 3 D**), **AW1** occupies hotspot 1 at the base of the
209 TrmD active site, where it satisfies the hydrogen-bond donor requirements by interacting with
210 the backbone amide oxygen atoms of Gly134 and Tyr136. The merged compound **AW1** also
211 orients its pyrazole nitrogen atom in the acceptor map in this region where it forms a hydrogen
212 bond with the backbone NH of Leu138 (**Figure 3 D**). The compound could be elaborated
213 further towards the methionine end of the active site and by further extension to the second
214 hotspot region at the top of the active site. The second hotspot is characterized by a large
215 hydrophobic patch surrounded by the acceptor region mediated by the backbone amide group
216 and side chain of Glu180. A second approach to fragment elaboration is by growing further
217 upwards from the hydrophobic region of hotspot 2 over to the donor region mainly mediated
218 by the backbone oxygen atom and side chains of Glu112 as illustrated in **Figure 3 D**.

219

220 **Structure-based lead optimization of merged compounds**

221 A structure-guided elaboration of the merged compound **AW1** (K_d 0.11 mM, LE 0.36, IC_{50}
222 0.23 mM) was carried out, initially utilizing the indole nitrogen as a vector for growth. The
223 addition of a 2-picolyl moiety successfully increased the affinity of **AW1** by an order of
224 magnitude in compound **AW2** (K_d 12 μ M, LE 0.30, IC_{50} 33 μ M) (**Table 1**). The methylene

225 linker attached to the indole nitrogen of **AW2** allowed the added pyridyl ring to occupy the
226 region defined by Pro85, Glu112, Val137, Arg154 and Glu180 (**Figures 3E & 4A**).

227 The affinity of **AW2** was further improved by the addition of a nitrile group on the 4-position
228 of its pyrazole ring, extending into the narrow space between residues ⁸³PTP⁸⁵ of the cover
229 loop and ¹³¹VSI¹³³ of the bottom loop respectively (**Figure 4 A & B**). **AW3** (K_d 0.50 μ M, LE
230 0.36, IC_{50} 0.31 μ M) was a significant improvement on **AW2**, with the addition of two heavy
231 atoms affording a 25-fold decrease in K_d (12 to 0.50 μ M), increasing the ligand efficiency to
232 the level of the original merged compound **AW1** (0.36), and a 100-fold decrease in IC_{50} (33 to
233 0.31 μ M) (**Table 1**). The X-ray crystal structure of TrmD in complex with **AW3** shows that
234 the original fragment contacts have been retained, with the **AW3** aminopyrazole ring orienting
235 itself in a similar manner to **AW1** and retaining its hydrogen bonding contacts to the side chain
236 of Ser132 and backbones of Gly134, Tyr136 and Leu138. In addition, the nitrile group of **AW3**
237 seems to have strengthened the interactions at the active site region between residues ⁸³PTP⁸⁵
238 and ¹³¹VSI¹³³ by engaging in an additional hydrogen bond contact with the backbone NH of
239 Ile133 (**Figure 4B**).

240 Further elaboration was carried out from the 5-position of the pyridyl ring of **AW3** through the
241 attachment of a pyrrolidinyl ring via another methylene linker, with **AW4** (K_d 92 nM, LE 0.34)
242 affording an additional 5-fold improvement in affinity (**Table 1**). Modification of the scaffold
243 of **AW4** by replacement of its pyridyl ring with a phenyl ring in **AW5** (K_d 27 nM, LE 0.34,
244 IC_{50} 30 nM) was tolerated with a greater than three-fold improvement in affinity (92 to 27 nM)
245 and an increase in ligand efficiency (0.32 to 0.34). The X-ray crystal structure of **AW5** shows
246 the pyrrolidinyl ring occupying the binding site in two conformations, depending on the active
247 site, thereby engaging either Glu112 or Glu180 in an electrostatic interaction (**Figure 4 C &**
248 **D**). The removal of the nitrile group on the pyrazole ring of **AW5** in compound **AW6** (K_d 0.49
249 μ M, LE 0.31, IC_{50} 1.4 μ M) (**Figure 5A**), had a detrimental impact on both affinity and

250 performance in the biochemical assay, demonstrating the importance of extension of this
251 substituent into the cavity between residues ⁸³PTP⁸⁵ of the cover loop and ¹³¹VSI¹³³ of the
252 bottom loop. Exploration of the active site region bordered by the Ala176 to Glu180 loop
253 through replacement of the pyrrolidinyl ring of **AW5** with an *N*-methyl piperazinyl motif in
254 **AW7** (K_d 73 nM, LE 0.30, IC₅₀ 69 nM) showed a slight worsening of both affinity and IC₅₀,
255 possibly due to the slight change (0.3 Å) in the position of the nitrile group in comparison to
256 that of **AW5**, thereby diminishing the hydrogen bonding contact with the backbone amide of
257 Thr84 (**Figure 5 B & S8**).

258

259 **TrmD lead compounds have anti-mycobacterial activity**

260 The compounds were further examined for their ability to inhibit bacterial growth. While the
261 initial fragment hits of TrmD and the early stage compounds elaborated from the fragments
262 exhibited low levels of growth inhibition up to 250 μM (data not shown), compounds in later
263 stages of development showed promising activity against *M. abscessus* and *M. tuberculosis*
264 (**Table 2**). The MICs of the TrmD lead compounds against *M. abscessus* were identical and
265 most of the lead molecules exhibited much higher inhibition against *M. tuberculosis* than *M.*
266 *abscessus* (**Table 2**). Surprisingly, **AW6**, in which the nitrile group of **AW5** was removed,
267 despite being the least active lead compound in the *in vitro* TrmD assays, showed similar MICs
268 when compared to the other two compounds. Additionally, the replacement of the pyrrolidinyl
269 ring of **AW5** with an *N*-methyl piperazinyl motif in **AW7** afforded a 2-fold improvement in
270 the MIC compared to **AW5** against *M. tuberculosis*, however this wasn't observed in *M.*
271 *abscessus* (**Table 2**). Sub-micromolar affinities were subsequently determined for **AW6** (K_d
272 0.90 μM) and **AW7** (K_d 0.33 μM) with TrmD from *M. tuberculosis* (**Figure S18 and S19**),
273 supporting both the MIC values against *M. tuberculosis* and the applicability of this lead series
274 to TrmD homologs from mycobacteria other than *M. abscessus*. The lead molecules **AW6** and

275 **AW7** were then tested against a wider panel of NTMs (**Table 2**). The obtained MICs revealed
276 that the compounds display limited inhibitory activity across most NTMs tested except for
277 *Mycobacterium terrae*, where MICs are better than for *M. abscessus*. Given the high percentage
278 sequence identity of TrmD across mycobacterial species (**Figure S1**), it was expected that
279 growth inhibition would be observed against some of these organisms. However, the variation
280 in MIC observed for our lead compounds is in line with the variation in drug susceptibility
281 profiles between mycobacterial species due to differential permeability, retention, and
282 metabolism of compounds (Li et al., 2013; Scherr et al., 2016).

283

284 **TrmD lead compounds kill intracellular *M. abscessus* and *M. leprae***

285 We assessed the cytotoxicity effect of **AW6** and **AW7** using lactate dehydrogenase (LDH)
286 release assay. At or below 150 μM , neither compound caused cellular toxicity on human
287 macrophages (**Figure S5**). The compounds were then evaluated in *M. abscessus*-infected
288 human macrophages. Both compounds showed activity in the macrophage infection model,
289 with **AW7** performing better than in the *in vitro* assays. At 25 μM **AW6** showed a ~82 %
290 decrease in CFUs while **AW7** at the same concentration showed a 95 % reduction in CFUs
291 compared to the no drug control after 48h incubation (**Figure 5C**). However, only **AW7**
292 demonstrated a bactericidal effect with a -0.8 log change after 48h incubation (**Figure 5C**).

293 The best lead molecule (**AW7**) was further tested against *M. leprae* maintained intracellularly
294 in murine bone marrow macrophage. Relative inhibition of β -oxidation rates were measured
295 using a radiorespirometry assay after 7 days of incubation. The results show that **AW7** at 6.2
296 μM was able to inhibit *M. leprae* radiorespirometry by ~54 % when compared to the no-drug
297 control and by ~89 % at 25 μM , which is similar to rifampicin inhibition at 2.4 μM (91%)
298 (**Figure 5D**). Axenically-maintained *M. leprae* showed only a 15% reduction of
299 radiorespirometry at 25 μM and no effect at 6.2 μM , following a similar trend to what was

300 observed for *M. abscessus* with the highest activity for the compound being observed in the
301 macrophage infection model (**Figure 5C, S6 & S7**).

302

303 **Discussion**

304 TrmD (tRNA-(N(1)G37) methyltransferase) is an essential tRNA modification enzyme in
305 bacteria that prevents translational frame-shift errors by methylation of a guanosine base at
306 position 37 of tRNAs containing G₃₆G₃₇ bases at the anti-codon region. This enzyme was found
307 to be essential in *M. tuberculosis* and other organisms but direct confirmation for *M. abscessus*
308 was lacking. This work has confirmed the essentiality of *trmD* for *M. abscessus* subsp.
309 *massiliense* growth, validating TrmD as a drug discovery target for this organism.

310 A FBDD effort targeting *M. abscessus* TrmD was undertaken by screening a library of 960
311 fragments by DSF and resulted in 53 preliminary hits. Of these, 27 were subsequently validated
312 by X-ray crystallographic studies of the TrmD-fragment complexes. The resulting fragments
313 can be classed into three clusters corresponding to their different binding modes in the TrmD
314 SAM binding site. The determination of high-resolution crystal structures informed structure-
315 guided drug discovery and allowed us to select and develop a series of compounds by merging
316 fragments **23** and **24**. Chemical elaboration of the merged compound **AW1** allowed the
317 synthesis of potent *M. abscessus* TrmD inhibitors. This was achieved through both the addition
318 of a nitrile group on the 4-position of the pyrazole ring and elaboration from the indole nitrogen.
319 This elaboration led to several low nanomolar *M. abscessus* TrmD inhibitors demonstrating a
320 significant improvement of *in vitro* affinity from the initial fragments.

321 The lead compounds reported in this work exhibited bactericidal effects on *M. abscessus*, *M.*
322 *tuberculosis*, and *M. terrae*. Furthermore, compound **AW7** showed bactericidal intracellular
323 activity against *M. abscessus* and was also a potent inhibitor of intracellular *M. leprae*. The
324 compounds reported here are the first TrmD inhibitors reported in the literature with strong

325 bactericidal activity against mycobacteria. However, we observe a poor correlation between
326 K_d/IC_{50} and MIC for the lead compounds, with **AW6**, the weakest of the lead compounds,
327 presenting similar MIC values to the other compounds against most of the species tested.
328 Furthermore, whilst the compounds have nanomolar affinities against TrmD from *M. abscessus*
329 and *M. tuberculosis*, and likely similar affinities for other mycobacterial TrmD given the very
330 high sequence identity shared between the TrmD orthologues (**Figure S1**), their MICs are ~35-
331 3000 fold worse across the NTMs tested. This poor correlation and variation across different
332 mycobacterial species suggests differential effects of compound permeability, retention, and/or
333 metabolism on *in vivo* activity. Similar results were found by others in a recent phenotypic
334 screen of 129 TB active and 271 non-TB active compounds against *M. abscessus* which
335 revealed that only a small subset (12 compounds) from the TB-active group and just one
336 compound from the non-TB active group were effective against *M. abscessus* (Low et al.,
337 2017). Nevertheless, our results with macrophage infection models, both with *M. leprae* and
338 *M. abscessus*, show the potential of these molecules to be further optimized. The preliminary
339 toxicity study of the lead molecules **AW6** and **AW7** using a lactate dehydrogenase (LDH)
340 assay further showed no significant cytotoxicity on primary human macrophages.
341 Most currently-used antibiotics that target microbial protein synthesis act either by interacting
342 with ribosomal sub-units (aminoglycosides, tetracyclines, macrolides etc) or *via* inhibiting
343 mRNA synthesis (rifamycins) and elongation (actinomycin) (Kohanski et al., 2010). This study
344 represents a proof of concept for the development of a new class of antibiotics targeting
345 bacterial tRNA modification with potent bactericidal activities. Furthermore, the results
346 presented in this work suggest the potential to develop novel mycobacterial drugs targeting
347 bacterial tRNA methylation by TrmD.

348

349

350 **Materials & Methods**

351 **Expression and purification of full length *M. abscessus* TrmD**

352 *E. coli* BL21 (DE3) strain containing AVA0421 plasmid with an N-His-3C Protease site-TrmD
353 full-length insert, kindly provided by the Seattle Structural Genomics Consortium, (Baugh et
354 al., 2015) was grown overnight at 37 °C in LB-media containing Ampicillin (100 µg/mL). This
355 seed stage culture was used to inoculate 6 shake flasks containing 1 L each of 2XYT media
356 with Ampicillin (100 µg/mL) until optical density (A_{600nm}) reached 0.6. The expression of
357 recombinant construct was induced by the addition of Isopropyl β-D-1-thiogalactopyranoside
358 (IPTG) to a final concentration of 0.5 mM and further allowed to grow at 18 °C for 16 h.

359 Isolation of cells & lysis: Cells were harvested by centrifugation at 4 °C for 20 min at 5000 g
360 and the pellet was re-suspended in buffer A (25 mM HEPES pH 7.5, 500 mM NaCl, 5%
361 Glycerol, 10 mM MgCl₂, 1 mM TCEP, 20 mM Imidazole). 0.1 % Triton (Sigma), 10 µg/mL
362 DNaseI, 5 mM MgCl₂, and 3 protease inhibitor cocktail tablets (New England Biolabs) were
363 added to the cell suspension. The cells were lysed in an Emulsiflex (Glen Creston) and clarified
364 the lysate by centrifugation at 4 °C for 40 min at 25,568 g.

365 Immobilized Metal Affinity Chromatography: The clarified lysate was filtered using a 0.45 µm
366 syringe filter and passed through a pre-equilibrated (with buffer A), 10 mL pre-packed nickel-
367 sepharose column (HiTrap IMAC FF, GE Healthcare). The column was washed with 5 column
368 volumes of buffer A and the bound protein was eluted as 4x 10 mL elutes using buffer B (25
369 mM HEPES pH 7.5, 500 mM NaCl, 5% Glycerol, 1 mM TCEP, 500 mM Imidazole). The
370 protein was analyzed on a 15% SDS-PAGE gel. Dialysis: Elutes from Hi-Trap IMAC column
371 were pooled, added 3C Protease in the ratio of 1: 50 mg (protease: protein) and subjected to
372 dialysis against 2 L of buffer C (25 mM HEPES pH 7.5, 500 mM NaCl, 5 % Glycerol, 1 mM
373 TCEP) overnight at 4 °C.

374 Protein, after overnight dialysis and cleavage of N-His tag, was passed through a pre-
375 equilibrated (buffer A) 5 mL HiTrap IMAC FF Nickel column (GE Healthcare).

376 Size Exclusion Chromatography: The flow through from the above column was concentrated
377 to 3 mL using a 10 kDa centrifugal concentrator (Sartorius Stedim) and loaded onto a pre-
378 equilibrated (with buffer D: 25 mM HEPES pH 7.5, 500 mM NaCl, 5% Glycerol) 120 mL
379 Superdex200 16/600 column (GE Healthcare). 2 mL fractions were collected and analyzed on
380 a 15% SDS-PAGE gel. Fractions corresponding to pure TrmD protein were pooled and
381 concentrated to 25 mg/mL, flash frozen in liquid nitrogen and stored at -80 °C. Identity of the
382 purified protein was further confirmed by MALDI fingerprinting.

383

384 **Crystallization of apo form of full length *M. abscessus* TrmD**

385 *M. abscessus* TrmD apo crystals were grown in 48-well sitting drop plates (Swiss CDI) in the
386 following condition: 0.08 mM Sodium cacodylate pH 5.8 to 6.8, 1–2 M Ammonium sulfate.
387 24 mg/mL of the protein in storage buffer (25 mM HEPES pH 7.5, 500 mM NaCl, 5%
388 Glycerol) at drop ratio 1 μ L: 1 μ L (protein: reservoir respectively) were set up and equilibrated
389 against 70 μ L reservoir.

390

391 **Soaking of TrmD native crystals with fragments and ligands**

392 Crystals for this experiment were grown at 19 °C in 48-well sitting drop plates (Swiss CDI) in
393 the following condition: 0.08 mM Sodium cacodylate pH 6.5 to 7.0, 1–2 M Ammonium sulfate,
394 20 mg/mL of the protein in storage buffer (25 mM HEPES pH 7.5, 500 mM NaCl, 5%
395 Glycerol) at drop ratio 1 μ L: 1 μ L were set up and equilibrated against 250 μ L reservoir. Further,
396 the crystals were picked and allowed to soak in a 4 μ L drop containing reservoir solution and
397 10 mM fragments/compound (in DMSO) which was then equilibrated against 700 μ L of the

398 corresponding reservoir solution overnight at 19 °C in 24-well hanging drop vapor diffusion
399 set up.

400

401 **Co-crystallization of TrmD protein with SAM/ SAH/ AW6/ AW7**

402 2-5 mM final concentration of compound in DMSO/water was added to 20 mg/mL of TrmD
403 protein, mixed and incubated for 2 h on ice. Crystals were grown in the following condition:
404 0.08mM Sodium cacodylate pH 6.5 to 7.0, 1–2 M Ammonium sulfate or in sparse matrix
405 screens: Wizard 1&2 (Molecular Dimensions), Wizard 3&4 (Molecular Dimensions), JCSG
406 +Suite (Molecular Dimensions). The crystallization drops were set up at a protein to reservoir
407 drop ratio of 0.3 μ L: 0.3 μ L, in 96-well (MRC2) sitting drop plate, using Mosquito
408 crystallization robot (TTP labtech) and the drops were equilibrated against 70 μ L of reservoir
409 at 19 °C.

410

411 **X-ray Data Collection and Processing**

412 The TrmD apo/ligand-bound crystals were cryo-cooled in mother liquor containing 27.5%
413 ethylene glycol. X-ray data sets were collected on I04, I02, I03, I04-1 or I24 beamlines at the
414 Diamond Light Source in the UK, using the rotation method at wavelength of 0.979 Å, Omega
415 start: 0°, Omega Oscillation: 0.1-0.2°, Total oscillation: 210-240°, Total images: 2100-2400,
416 Exposure time: 0.05-0.08 s. The diffraction images were processed using AutoPROC
417 (Vonrhein et al., 2011), utilizing XDS (Kabsch, 2010) for indexing, integration, followed by
418 POINTLESS (Evans, 2011), AIMLESS (Evans and Murshudov, 2013) and TRUNCATE
419 (French, 1978) programs from CCP4 Suite (Winn et al., 2011) for data reduction, scaling and
420 calculation of structure factor amplitudes and intensity statistics. All TrmD crystals belonged
421 to space group P2₁2₁2₁ and consisted of two protomers in the asymmetric unit.

422

423 **Structure Solution and refinement**

424 The *Mycobacterium abscessus* TrmD Apo structure was solved by molecular replacement
425 using PHASER (McCoy et al., 2007) with the atomic coordinates of *Mycobacterium abscessus*
426 TrmD at 1.7 Å (PDB entry: 3QUV Seattle Structural Genomics Consortium for Infectious
427 Diseases) as search model and TrmD ligand bound structures were solved by molecular
428 replacement with the atomic coordinates of the solved *Mycobacterium abscessus* TrmD Apo
429 structure (PDB entry: 6NVR) as search model. Structure refinement was carried out using
430 REFMAC (Murshudov et al., 2011) and PHENIX (Adams et al., 2010).

431 The models obtained were manually re-built using COOT interactive graphics program
432 (Emsley and Cowtan, 2004) and electron density maps were calculated with $2|F_o| - |F_c|$ and $|F_o|$
433 $- |F_c|$ coefficients. Positions of ligands and water molecules were located in difference electron
434 density maps and OMIT difference maps $|mF_o - DF_c|$ (Hodel, 1992) were calculated and
435 analysed to further verify positions of fragments and ligands. The corresponding statistics and
436 omit maps are presented in supplementary data **Table S1** and **Figure S8**.

437

438 **Differential scanning fluorimetry (DSF)**

439 DSF were carried out in a 96-well format with each well containing 25 µL of reaction mixture
440 of 10 µM TrmD protein in buffer (50 mM HEPES pH 7.5, 500 mM NaCl, 5% glycerol), 5 mM
441 compound, 5% DMSO and 5X Sypro orange dye. Appropriate positive (Protein, DMSO and
442 SAM) and negative (Protein, DMSO only) controls were also included. The measurements
443 were performed in a Biorad-CFX connect thermal cycler using the following program: 25 °C
444 for 10 mins followed by a linear increment of 0.5 °C every 30 sec to reach a final temperature
445 of 95 °C. The results were analyzed using Microsoft excel.

446

447

448 **Isothermal Titration Calorimetry (ITC)**

449 ITC experiments to quantify binding of ligands to TrmD were done as described in
450 (Whitehouse *et al.* 2019) using Malvern MicroCal iTC200 or Auto-iTC200 systems at 25 °C.
451 Titrations consisted of an initial injection (0.2 µL), discarded during data processing, followed
452 by either 19 (2 µL) or 39 (1 µL) injections separated by intervals of 60 – 150 seconds duration.
453 Protein was dialysed overnight at 4 °C in storage buffer (*M. abscessus* TrmD: 50 mM HEPES
454 pH 7.5, 500 mM NaCl, 5% glycerol; *M. tuberculosis* TrmD: 25 mM HEPES pH 7.5, 500 mM
455 NaCl). Sample cell and syringe solutions were prepared using the same storage buffer, with a
456 final DMSO concentration of 2 – 10% according to ligand solubility in the buffer. TrmD
457 concentrations of either 33 or 100 µM were used, with ligand to protein concentration ratios
458 ranging from 10-20:1. Control titrations without protein were also performed and subtracted
459 from ligand to protein titrations. Titrations were fitted with Origin software (OriginLab,
460 Northampton, MA, USA), using a one-site binding model with N fixed to 1 only for weakly
461 binding ligands. Titrations were typically performed once (n = 1), with multiple isotherms
462 obtained (n > 1) for key compounds of interest. K_d values are reported to 2 significant figures.
463 Error provided by Origin software due to model fit is reported when n = 1, whereas standard
464 deviation is reported when n > 1.

465

466 **Biochemical activity assays**

467 Assays for quantifying TrmD methylation reactions were carried out in 20 uL reactions
468 consisting of 6.25 µM SAM, 0.1 µM TrmD and 6.25 µM tRNA in the presence of 0-500 µM
469 compounds in serial dilutions using assay buffer containing 50 mM Tris-HCl pH 7.5, 10 mM
470 MgCl₂, 24 mM NH₄Cl, 5% DMSO and 1 mM DTT in nuclease free water. tRNA sequences
471 were identified from the *M. abscessus* genome sequence using tRNAscan-SE algorithm, (Lowe
472 and Chan, 2016; Lowe and Eddy, 1997). The substrate tRNA^{Pro} for the assay was purchased

473 commercially from Integrated DNA technologies (USA). The reactions were carried out for 1
474 h at room temperature followed by addition of 20 mM EDTA to stop the reactions. Each of the
475 20 uL samples were diluted ten-fold with the UPLC mobile phase solvent A (0.1% formic acid
476 in water), centrifuged for 10 min at 13,000 g, to remove any precipitates, and the supernatant
477 was aliquoted into 96-well plates. 40 uL samples were then injected into Acquity UPLC
478 (Waters) T3 1.8 μ M column and eluted using a gradient elution consisting of Mobile Phase A:
479 0.1% formic acid in water and mobile phase B: 0.1% formic acid in 100% methanol for 4 min.
480 The absorbance was monitored using a photodiode array (PDA) detector (Waters) at
481 wavelength range of λ : 220– 500 nm. All reactions were carried out in triplicate. The blank
482 corrected data were analysed using Microsoft excel and non-linear regression analysis for IC₅₀
483 determination were done using Graph Pad prism version 7.00, GraphPad Software, La Jolla
484 California USA.

485

486 **Mycobacterial strains used and MIC measurements**

487 The following mycobacterial strains were used: *Mycobacterium abscessus subspecies*
488 *abscessus* (ATCC 19977) transformed with pmv310 plasmid expressing Lux ABDCE operon,
489 grown in Middlebrook 7H9 broth supplemented with ADC (Sigma, UK) and *M. tuberculosis*
490 Δ leuD Δ panCD (Bleupan) (Sampson et al., 2004) transformed with pSMT1 expressing Lux
491 AB and GFP, grown in Middlebrook 7H9 broth supplemented with 0.5% glycerol, 0.05%
492 Tween 80 (removed for 24 h prior to experiments), 10% OADC (BD), 0.05 mg/ml L-leucine,
493 and 0.024 mg/ml calcium pantothenate, Hygromycin and Zeocin (removed for 24 h prior to
494 experiments). All the other NTM strains are clinical isolates. Minimum Inhibitory
495 Concentrations (MIC) were determined for mycobacteria according to the Clinical and
496 Laboratory Standards Institute (CLSI) method M07-A9. Briefly, mycobacteria were grown to
497 optical density (A_{600nm}) of 0.2-0.3 in liquid culture and 1×10^5 bacteria were added to each well

498 of 96-well plates containing serial dilutions of compound (400, 200, 100, 50, 25, 12.5, 6.3, 3.1,
499 1.6, 0.8, 0.4, 0 μM), in triplicate wells per condition, and incubated at 37 °C until growth was
500 seen in the control wells. MIC measurements using *M. tuberculosis* H37Rv were performed as
501 reported in. *M. tuberculosis* H37Rv was grown in Middlebrook 7H9 base containing 14 mg/L
502 dipalmitoyl phosphatidylcholine (DPPC), 0.81 g/L NaCl, 0.3 g/L casitone, and 0.05%
503 Tyloxapol. H37Rv was grown and diluted to a similar inoculum size as mentioned above prior
504 to exposure to serial dilutions of compounds (starting at 100 μM), and the plates were incubated
505 at 37°C for two weeks. The MIC value was determined as the last well which showed no
506 bacterial growth.

507

508 **Expression and purification of *M. tuberculosis* TrmD**

509 A colony of *E. coli* strain ANG3685 (XL1 Blue pET23b-His6-trmDTB) kindly provided by
510 the research group of Professor Angelika Gründling at Imperial College London (Zhang et al.,
511 2017), was transferred to LB media (5 mL) with ampicillin (100 $\mu\text{g mL}^{-1}$) and incubated
512 overnight (37 °C, 160 rpm). The resultant material was processed with a GeneJET™ Plasmid
513 Miniprep Kit (Thermo Scientific™) to obtain plasmid (30 ng μL^{-1} , $A_{260\text{nm}}/A_{280\text{nm}}$ 1.87), with
514 identity confirmed by Sanger sequencing (DNA Sequencing Facility, Department of
515 Biochemistry, University of Cambridge).

516 The isolated plasmid was used to transform *E. coli* strain BL21 (DE3), with a colony transferred
517 to LB media (20 mL) with ampicillin (100 $\mu\text{g mL}^{-1}$) and incubated overnight (37 °C, 160 rpm).

518 The starter culture was used to inoculate 2 flasks, each containing LB media (1 L) with
519 ampicillin (100 $\mu\text{g mL}^{-1}$), with incubation (37 °C, 200 rpm) until an optical density ($A_{600\text{nm}}$) of
520 0.5 was reached. Protein expression was induced by the addition of isopropyl β -D-1-
521 thiogalactopyranoside (0.5 mM), followed by overnight incubation (20 °C, 200 rpm). Cells
522 were harvested by centrifugation (4 °C, 4000 g, 20 minutes), then frozen.

523 The cells were resuspended in 50 mL lysis buffer (50 mM HEPES pH 7.4, 1 M NaCl, 25 mM
524 imidazole, 5 mM mercaptoethanol) with a tablet of cOmplete™ Protease Inhibitor Cocktail
525 (Roche). The suspension was sonicated (10 minutes: 10 seconds on/ 20 seconds off),
526 centrifuged (4 °C, 30000 g, 20 minutes) and filtered (0.45 µm). The resultant lysate was loaded
527 onto a 7.5 mL nickel Sepharose™ fast flow column (GE Healthcare), pre-equilibrated with
528 lysis buffer. The column was washed with 5 column volumes of buffer A (25 mM HEPES pH
529 7.5, 500 mM NaCl, 20 mM imidazole, 5 mM mercaptoethanol) and eluted with buffer B (25
530 mM HEPES pH 7.5, 500 mM NaCl, 500 mM imidazole, 5 mM mercaptoethanol) in 7 x 5 mL
531 aliquots. Protein-containing aliquots, as determined by SDS-PAGE, were combined and
532 concentrated (10 kDa cutoff) to a volume of 7 mL, then loaded onto a Superdex 75 Hiload™
533 16/60 column (GE Healthcare) pre-equilibrated with filtration buffer (25 mM HEPES pH 7.5,
534 500 mM NaCl, 5 mM mercaptoethanol). Protein-containing fractions, as determined by SDS-
535 PAGE, were combined and concentrated (10 kDa cutoff) to 14.4 mg mL⁻¹ (5.0 mg L⁻¹ yield),
536 then flash-frozen in liquid nitrogen and stored at -80 °C. The identity of the protein was
537 confirmed by LCMS analysis.

538

539 **Macrophage infection study**

540 Blood samples were donated by healthy volunteers who had undertaken informed consent in
541 accordance with local Research Ethics Committee approval. Peripheral blood mononuclear
542 cells were isolated from citrated peripheral blood samples by density gradient separation using
543 Lympholyte (Cedarlane Labs), and subsequent CD14⁺ positive selection using the MACS
544 Miltenyi Biotec Human CD14 microbead protocol (Miltenyi Biotec). CD14⁺ cells were
545 differentiated in to macrophages using recombinant human granulocyte-macrophage colony-
546 stimulating factor (200 ng/mL GM-CSF) and recombinant human interferon gamma (50 ng/ml
547 IFNγ) (Peprotech) in standard tissue culture DMEM media containing fetal calf serum,

548 penicillin and streptomycin. Following removal of antibiotics, macrophages were infected at a
549 multiplicity of infection of 10:1 with *M abscessus* 19977 for 2 h, washed in sterile phosphate
550 buffered saline, and then incubated in DMEM media with FCS and 25 μ M of compound for
551 24 and 48 h. At the given time points, supernatant was saved for cell cytotoxicity studies, and
552 *M abscessus* survival within the macrophages calculated by macrophage lysis in sterile water,
553 and colony forming unit calculation on Columbia Blood Agar plates (VWR BDH).

554

555 **Cytotoxicity**

556 Lactate dehydrogenase (LDH) was measured as a biomarker for cellular cytotoxicity using the
557 Pierce LDH Cytotoxicity Assay Kit. Cell supernatant was measured at 2, 24 and 48 hours post
558 infection according to the kit protocol.

559

560 **Nude mouse derived *M. leprae***

561 *Mycobacterium leprae* (isolate Thai-53) was maintained in serial passage in the foot pads of
562 athymic nude mice (Envigo, US.). Mice were inoculated in the plantar surface of both hind
563 feet with 5×10^7 fresh, viable nude mice derived *M. leprae*. When the mouse foot pads became
564 moderately enlarged (at \sim 5 - 6 months), they were harvested for intracellular *M. leprae* as
565 described previously (Truman and Krahenbuhl, 2001), washed by centrifugation, re-suspended
566 in medium, enumerated by direct count of acid fast bacilli according to Shepard's method
567 (Shepard and McRae, 1968), held at 4 °C pending quality control tests for contamination and
568 viability (Truman and Krahenbuhl, 2001). Freshly harvested bacilli were always employed in
569 experiments within 24 h of harvest.

570

571 ***M. leprae* axenic culture**

572 Freshly harvested nude mouse foot pad derived *M. leprae* were suspended in modified 7H12

573 medium, **AW7** was added at different concentrations (100 μM – 6.25 μM) and were incubated
574 for 7 days at 33 °C. Media only and rifampin (Sigma, USA) at 2.4 μM were used as negative
575 and positive controls. Following incubation aliquots of **AW7** treated and control *M. leprae*
576 were processed for radiorespirometry (RR) as described previously (Lahiri et al., 2005).

577

578 ***M. leprae* macrophage culture**

579 Bone marrow cells were obtained aseptically from both femurs of female BALB/c mice and
580 cultured on plastic cover slips in Dulbecco modified Eagle media (DMEM, Life Technologies,
581 USA) supplemented with 10% v/v fetal calf serum (Life Technologies), 25 mM/L HEPES
582 (Sigma, USA), 2 mM/L glutamine (Sigma, USA), 50 $\mu\text{g}/\text{mL}$ ampicillin (Sigma, USA) and 10
583 ng/mL of recombinant murine macrophages colony stimulating factor (R &D Systems, USA)
584 for 6 - 7 days at 37°C and 5% CO₂. The cells were infected with freshly harvested nude mice
585 foot pad derived live *M. leprae* at a multiplicity of infection (MOI) of 20:1 overnight at 33 °C
586 and then washed to remove extracellular bacteria. **AW7** was added at different concentrations
587 (100 μM – 6.25 μM) and the cells were incubated for 7 days at 33°C. Media only and rifampicin
588 at 2.4 μM were used as negative and positive controls. **AW7** treated and control cells were
589 lysed with sodium dodecyl sulfate (SDS, 0.1% w/v, Sigma, USA) and the intracellular *M.*
590 *leprae* processed for radiorespirometry (Lahiri et al., 2010).

591

592 **Radiorespirometry**

593 Metabolism of a suspension of *M. leprae* was measured by evaluating the oxidation of
594 ¹⁴C-palmitic acid to ¹⁴CO₂ by radiorespirometry as described previously (Franzblau, 1988).
595 Levels of captured ¹⁴CO₂ is proportional to the rate of ¹⁴C-palmitic acid oxidation and used as
596 an indicator of *M. leprae* viability. In the present study the 7th day cumulative counts per
597 minute (CPM) were recorded and percentage inhibition of metabolism determined as compared

598 to no drug control. Statistical significance between treatment groups and no drug control were
599 determined by Student's t-test and $P < 0.05$ is considered as significant.

600

601 **Figure Legends**

602 **Figure 1: A)** TrmD reaction scheme illustrated with tRNA^{Leu} CAG as substrate. The
603 methylation of G37 base adjacent to the anti-codon region leading to N1-methyl-guanosine 37
604 is mediated by methyl donor *S*-adenosyl-L-methionine, which in turn gets converted into *S*-
605 adenosyl-L-homocysteine **B)** Allelic replacement at the *trmD* locus of *M. abscessus*. Candidate
606 *trmD* mutants were analysed by PCR using a set of primers annealing outside the allelic
607 exchange substrate. Lanes 1 to 6 show *M. abscessus subsp. massiliense* CIP108297 clones
608 harboring the pMV306H::*trmD* plasmid whose endogenous chromosomal *trmD* locus was
609 replaced by the Str cassette (expected size of the PCR fragment is 4,200 bp). Lane 7 shows the
610 amplification product of the *trmD* locus in wild-type *M. abscessus subsp. massiliense*
611 CIP108297 (expected size of the PCR fragment is 2,571 bp). MWM, molecular weight marker.
612 **C)** TrmD homodimer (PDB code 6NVR) with domain architecture illustrated. Protomers 1 and
613 2 are represented in brown and green ribbon diagrams respectively. **D)** TrmD protomer is
614 coloured and illustrated based on secondary structure elements. The disordered inter-domain
615 linker is shown as black dotted lines.

616

617 **Figure 2: A)** Structural superposition of TrmD apo form (white) and TrmD SAM bound form
618 (light blue), PDB codes 6NVR and 6NW6 respectively **B)** the trefoil-knot active site of TrmD
619 involving: cover loop (residues 84-87) shown in dark blue and bottom loop (residues 132-140)
620 in magenta and wall loop (residues 109-115) in green and the conformational flip of the wall
621 loop (residues ¹⁰⁹GRYEGID¹¹⁵) upon SAM (light blue stick) binding are illustrated. The
622 residues corresponding to each loop region are also shown as line representation. **C)** Three

623 representative fragment hits from each cluster, fragment **14** (PDB Code 6QOK) coloured in
624 blue, fragment **20** (PDB Code 6QOQ) in green and fragment **8** (PDB Code 6QOE) in salmon
625 respectively, occupying the TrmD SAM binding site. Major Hydrogen bonds and electrostatic
626 interactions are depicted in black and purple dotted lines respectively. **D)** Hot spot map
627 contoured at 14 of TrmD active site superposed with crystal structure of TrmD in complex with
628 merged compound **AW1** (light blue stick). Donor, acceptor and hydrophobic regions of the
629 map are depicted as blue, red and yellow regions respectively. Amino acid residues contributing
630 towards interactions in each hotspot map region are shown as brown stick representation. The
631 arrows indicate two potential ways of fragment elaboration.

632

633 **Figure 3:** Fragment merging approach. **A)** Structural superposition of TrmD (grey) in complex
634 with fragments **23** (green) and **24** (beige) – PDB Codes 6QOT & 6QOU, showing binding
635 mode and interactions at the SAM site **B)** merged compound **AW1** (light blue), PDB Code
636 6QQS, showing binding mode at the SAM site. The corresponding amino acid interactions are
637 illustrated in dotted lines and **C)** the overall scheme of fragment merging.

638

639 **Figure 4:** X-ray crystal structure of TrmD (grey) in complex with compounds **A)** **AW2** (green
640 stick), PDB Code 6QQX **(B)** **AW3** (yellow stick), PDB Code 6QQY **(C)** **AW5** at protomer 1,
641 (blue stick), PDB Code 6QR6 and **(D)** **AW5** at protomer 2 (blue stick), PDB Code 6QR6,
642 showing binding mode at the SAM site. The corresponding amino acid interactions are
643 illustrated with Hydrogen bonds, π -interactions and electrostatic contacts depicted in black,
644 green and purple dotted lines respectively.

645

646 **Figure 5:** X-ray crystal structure of TrmD (grey) in complex with compound **A)** **AW6** (lime),
647 PDB Code 6QR5 **B)** **AW7** (green), PDB Code 6QR8, showing binding mode at the SAM site.

648 The corresponding amino acid interactions are illustrated with Hydrogen bonds, π -interactions
649 and electrostatic contacts depicted in black, green and purple dotted lines respectively. **C)**
650 Growth inhibition study of lead compounds **AW6** & **AW7** in *M. abscessus* infected human
651 macrophages over a 48 h period. Data represented as fold change in log (CFU/ml) from 2 h
652 infection in the absence of any drug. Fold change in log (CFU/ml) following 48 h infection
653 with no drug and with 25 μ M **AW7** are statistically significant ($P < 0.05$) in comparison to that
654 in the presence of **AW6** 48 h post infection ($P = 0.1437$) implying that **AW6** is bacteriostatic
655 and **AW7** is bactericidal for *M. abscessus*. **D)** Intracellular *M. leprae* palmitic acid oxidation
656 rate (radiorespirometry) in the presence of different concentrations of **AW7** for 7 days. 7th day
657 cumulative counts per minute (CPM) were recorded and percentage inhibition of metabolism
658 determined as compared to no drug control. **AW7** concentrations, in mM, are shown in
659 parenthesis and rifampin (RMP) was used at 2.4 mM. * - Inhibition is statistically significant
660 ($P < 0.05$) compared to no drug control.

661

662

663

664

665

666

667

668

669

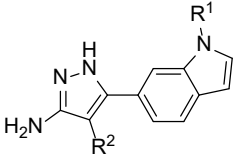
670

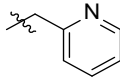
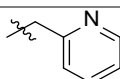
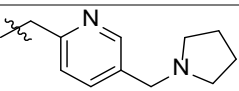
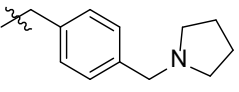
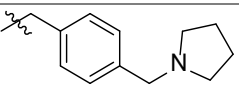
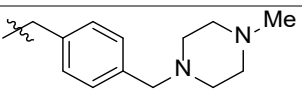
671

672

673 **Table 1: Summary of structure-guided optimization of merged compound AW1**

674



Compound	Structure		K _d (μM)	LE (kcal/ mol/ heavy atom)	IC ₅₀ (μM)
	R ¹	R ²			
AW1	H	H	110 ± 11	0.36	230 ± 29
AW2		H	12 ± 1	0.30	33 ± 4
AW3		CN	0.50 ± 0.14	0.36	0.31 ± 0.01
AW4		CN	0.092 ± 0.018	0.32	ND
AW5		CN	0.027 ± 0.004	0.34	0.030 ± 0.003
AW6		H	0.49 ± 0.21	0.31	1.4 ± 0.1
AW7		CN	0.073 ± 0.030	0.30	0.069 ± 0.007

675

676

677 **Table 2: Minimum inhibitory concentration (MIC) values of TrmD compounds across**
 678 various mycobacterial species and strains

No	MIC (μM)							
	<i>M. abscessus</i> 19977	<i>M. tuberculosis</i> Bluepan	<i>M. tuberculosis</i> H37Rv	<i>M. chelonae</i>	<i>M. fortuitum</i>	<i>M. goodnae</i>	<i>M. terrae</i>	<i>M. avium</i>
AW5	50	50	12.5	ND	ND	ND	ND	ND
AW6	50	25	6.3	100	100	100	100	200
AW7	50	25	6.3	100	100	100	25	100

679

680

681

682

References

- 683
684
685 Adams, P.D., Afonine, P.V., Bunkoczi, G., Chen, V.B., Davis, I.W., Echols, N., Headd, J.J.,
686 Hung, L.W., Kapral, G.J., Grosse-Kunstleve, R.W., *et al.* (2010). PHENIX: a comprehensive
687 Python-based system for macromolecular structure solution. *Acta crystallographica Section D,*
688 *Biological crystallography* *66*, 213-221.
- 689 Ahn, H.J., Kim, H.W., Yoon, H.J., Lee, B.I., Suh, S.W., and Yang, J.K. (2003). Crystal
690 structure of tRNA(m1G37)methyltransferase: insights into tRNA recognition. *The EMBO*
691 *journal* *22*, 2593-2603.
- 692 Anantharaman, V., Koonin, E.V., and Aravind, L. (2002). SPOUT: a class of
693 methyltransferases that includes spoU and trmD RNA methylase superfamilies, and novel
694 superfamilies of predicted prokaryotic RNA methylases. *J Mol Microbiol Biotechnol* *4*, 71-75.
- 695 Bar-On, O., Mussaffi, H., Mei-Zahav, M., Prais, D., Steuer, G., Stafler, P., Hananya, S., and
696 Blau, H. (2015). Increasing nontuberculous mycobacteria infection in cystic fibrosis. *Journal*
697 *of cystic fibrosis : official journal of the European Cystic Fibrosis Society* *14*, 53-62.
- 698 Baugh, L., Phan, I., Begley, D.W., Clifton, M.C., Armour, B., Dranow, D.M., Taylor, B.M.,
699 Muruthi, M.M., Abendroth, J., Fairman, J.W., *et al.* (2015). Increasing the structural coverage
700 of tuberculosis drug targets. *Tuberculosis (Edinb)* *95*, 142-148.
- 701 Bjork, G.R., Jacobsson, K., Nilsson, K., Johansson, M.J., Bystrom, A.S., and Persson, O.P.
702 (2001). A primordial tRNA modification required for the evolution of life? *The EMBO journal*
703 *20*, 231-239.
- 704 Bjork, G.R., Wikstrom, P.M., and Bystrom, A.S. (1989). Prevention of translational
705 frameshifting by the modified nucleoside 1-methylguanosine. *Science* *244*, 986-989.
- 706 Christian, T., Sakaguchi, R., Perlinska, A.P., Lahoud, G., Ito, T., Taylor, E.A., Yokoyama, S.,
707 Sulkowska, J.I., and Hou, Y.M. (2016). Methyl transfer by substrate signaling from a knotted
708 protein fold. *Nat Struct Mol Biol* *23*, 941-948.
- 709 DeJesus, M.A., Gerrick, E.R., Xu, W., Park, S.W., Long, J.E., Boutte, C.C., Rubin, E.J.,
710 Schnappinger, D., Ehrt, S., Fortune, S.M., *et al.* (2017). Comprehensive Essentiality Analysis
711 of the Mycobacterium tuberculosis Genome via Saturating Transposon Mutagenesis. *MBio* *8*.
- 712 Emsley, P., and Cowtan, K. (2004). Coot: model-building tools for molecular graphics. *Acta*
713 *crystallographica Section D, Biological crystallography* *60*, 2126-2132.
- 714 Erlanson, D.A., Fesik, S.W., Hubbard, R.E., Jahnke, W., and Jhoti, H. (2016). Twenty years
715 on: the impact of fragments on drug discovery. *Nature reviews Drug discovery* *15*, 605-619.
- 716 Evans, P.R. (2011). An introduction to data reduction: space-group determination, scaling and
717 intensity statistics. *Acta crystallographica Section D, Biological crystallography* *67*, 282-292.

- 718 Evans, P.R., and Murshudov, G.N. (2013). How good are my data and what is the resolution?
719 *Acta crystallographica Section D, Biological crystallography* 69, 1204-1214.
- 720 Floto, R.A., Olivier, K.N., Saiman, L., Daley, C.L., Herrmann, J.L., Nick, J.A., Noone, P.G.,
721 Bilton, D., Corris, P., Gibson, R.L., *et al.* (2016). US Cystic Fibrosis Foundation and European
722 Cystic Fibrosis Society consensus recommendations for the management of non-tuberculous
723 mycobacteria in individuals with cystic fibrosis. *Thorax* 71 *Suppl* 1, i1-22.
- 724 Floyd, K., Glaziou, P., Zumla, A., and Raviglione, M. (2018). The global tuberculosis epidemic
725 and progress in care, prevention, and research: an overview in year 3 of the End TB era. *The*
726 *Lancet Respiratory medicine* 6, 299-314.
- 727 Franzblau, S.G. (1988). Oxidation of palmitic acid by *Mycobacterium leprae* in an axenic
728 medium. *J Clin Microbiol* 26, 18-21.
- 729 French, S.W., K., (1978). On the treatment of negative intensity observations. *Acta Cryst* A34,
730 517-525.
- 731 Goto-Ito, S., Ito, T., Kuratani, M., Bessho, Y., and Yokoyama, S. (2009). Tertiary structure
732 checkpoint at anticodon loop modification in tRNA functional maturation. *Nat Struct Mol Biol*
733 16, 1109-1115.
- 734 Goto-Ito, S., Ito, T., and Yokoyama, S. (2017). Trm5 and TrmD: Two Enzymes from Distinct
735 Origins Catalyze the Identical tRNA Modification, m(1)G37. *Biomolecules* 7.
- 736 Griffin, J.E., Gawronski, J.D., Dejesus, M.A., Ioerger, T.R., Akerley, B.J., and Sasseti, C.M.
737 (2011). High-resolution phenotypic profiling defines genes essential for mycobacterial growth
738 and cholesterol catabolism. *PLoS Pathog* 7, e1002251.
- 739 Hajduk, P.J., Huth, J.R., and Tse, C. (2005). Predicting protein druggability. *Drug discovery*
740 *today* 10, 1675-1682.
- 741 Hill, P.J., Abibi, A., Albert, R., Andrews, B., Gagnon, M.M., Gao, N., Grebe, T., Hajec, L.I.,
742 Huang, J., Livchak, S., *et al.* (2013). Selective inhibitors of bacterial t-RNA-(N(1)G37)
743 methyltransferase (TrmD) that demonstrate novel ordering of the lid domain. *Journal of*
744 *medicinal chemistry* 56, 7278-7288.
- 745 Hodel, A., Kim, S.-H. & Brünger, A. T., (1992). Model bias in macromolecular crystal
746 structures. *Acta Cryst* A 48, 851-858.
- 747 Hori, H. (2017). Transfer RNA methyltransferases with a SpoU-TrmD (SPOUT) fold and their
748 modified nucleosides in tRNA. *Biomolecules* 7.
- 749 Ichihara, O., Shimada, Y., and Yoshidome, D. (2014). The importance of hydration
750 thermodynamics in fragment-to-lead optimization. *ChemMedChem* 9, 2708-2717.

- 751 Ito, T., Masuda, I., Yoshida, K., Goto-Ito, S., Sekine, S., Suh, S.W., Hou, Y.M., and Yokoyama,
752 S. (2015). Structural basis for methyl-donor-dependent and sequence-specific binding to tRNA
753 substrates by knotted methyltransferase TrmD. *Proceedings of the National Academy of*
754 *Sciences of the United States of America* *112*, E4197-4205.
- 755 Kabsch, W. (2010). XDS. *Acta crystallographica Section D, Biological crystallography* *66*,
756 125-132.
- 757 Koh, C.S., Madireddy, R., Beane, T.J., Zamore, P.D., and Korostelev, A.A. (2017). Small
758 methyltransferase RlmH assembles a composite active site to methylate a ribosomal
759 pseudouridine. *Scientific reports* *7*, 969.
- 760 Kohanski, M.A., Dwyer, D.J., and Collins, J.J. (2010). How antibiotics kill bacteria: from
761 targets to networks. *Nat Rev Microbiol* *8*, 423-435.
- 762 Lahiri, R., Randhawa, B., and Krahenbuhl, J. (2005). Application of a viability-staining method
763 for *Mycobacterium leprae* derived from the athymic (nu/nu) mouse foot pad. *J Med Microbiol*
764 *54*, 235-242.
- 765 Lahiri, R., Randhawa, B., and Krahenbuhl, J.L. (2010). Infection of mouse macrophages with
766 viable *Mycobacterium leprae* does not induce apoptosis. *J Infect Dis* *201*, 1736-1742.
- 767 Li, G., Lian, L.L., Wan, L., Zhang, J., Zhao, X., Jiang, Y., Zhao, L.L., Liu, H., and Wan, K.
768 (2013). Antimicrobial susceptibility of standard strains of nontuberculous mycobacteria by
769 microplate Alamar Blue assay. *PLoS One* *8*, e84065.
- 770 Low, J.L., Wu, M.L., Aziz, D.B., Laleu, B., and Dick, T. (2017). Screening of TB Actives for
771 Activity against Nontuberculous Mycobacteria Delivers High Hit Rates. *Frontiers in*
772 *microbiology* *8*, 1539.
- 773 Lowe, T.M., and Chan, P.P. (2016). tRNAscan-SE On-line: integrating search and context for
774 analysis of transfer RNA genes. *Nucleic acids research* *44*, W54-57.
- 775 Lowe, T.M., and Eddy, S.R. (1997). tRNAscan-SE: a program for improved detection of
776 transfer RNA genes in genomic sequence. *Nucleic acids research* *25*, 955-964.
- 777 McCoy, A.J., Grosse-Kunstleve, R.W., Adams, P.D., Winn, M.D., Storoni, L.C., and Read,
778 R.J. (2007). Phaser crystallographic software. *J Appl Crystallogr* *40*, 658-674.
- 779 Mendes, V., and Blundell, T.L. (2016). Targeting tuberculosis using structure-guided
780 fragment-based drug design. *Drug discovery today*.
- 781 Murray, C.W., Erlanson, D.A., Hopkins, A.L., Keseru, G.M., Leeson, P.D., Rees, D.C.,
782 Reynolds, C.H., and Richmond, N.J. (2014). Validity of ligand efficiency metrics. *ACS*
783 *medicinal chemistry letters* *5*, 616-618.

- 784 Murshudov, G.N., Skubak, P., Lebedev, A.A., Pannu, N.S., Steiner, R.A., Nicholls, R.A., Winn,
785 M.D., Long, F., and Vagin, A.A. (2011). REFMAC5 for the refinement of macromolecular
786 crystal structures. *Acta crystallographica Section D, Biological crystallography* *67*, 355-367.
- 787 Radoux, C.J., Olsson, T.S., Pitt, W.R., Groom, C.R., and Blundell, T.L. (2016). Identifying
788 Interactions that Determine Fragment Binding at Protein Hotspots. *Journal of medicinal*
789 *chemistry* *59*, 4314-4325.
- 790 Sampson, S.L., Dascher, C.C., Sambandamurthy, V.K., Russell, R.G., Jacobs, W.R., Jr., Bloom,
791 B.R., and Hondalus, M.K. (2004). Protection elicited by a double leucine and pantothenate
792 auxotroph of *Mycobacterium tuberculosis* in guinea pigs. *Infect Immun* *72*, 3031-3037.
- 793 Sasseti, C.M., Boyd, D.H., and Rubin, E.J. (2003). Genes required for mycobacterial growth
794 defined by high density mutagenesis. *Mol Microbiol* *48*, 77-84.
- 795 Scherr, N., Pluschke, G., and Panda, M. (2016). Comparative Study of Activities of a Diverse
796 Set of Antimycobacterial Agents against *Mycobacterium tuberculosis* and *Mycobacterium*
797 *ulcerans*. *Antimicrob Agents Chemother* *60*, 3132-3137.
- 798 Shepard, C.C., and McRae, D.H. (1968). A method for counting acid-fast bacteria. *Int J Lepr*
799 *Other Mycobact Dis* *36*, 78-82.
- 800 Sood, G., and Parrish, N. (2017). Outbreaks of nontuberculous mycobacteria. *Curr Opin Infect*
801 *Dis* *30*, 404-409.
- 802 Thomas, S.E., Mendes, V., Kim, S.Y., Malhotra, S., Ochoa-Montano, B., Blaszczyk, M., and
803 Blundell, T.L. (2017). Structural Biology and the Design of New Therapeutics: From HIV and
804 Cancer to Mycobacterial Infections: A Paper Dedicated to John Kendrew. *Journal of molecular*
805 *biology* *429*, 2677-2693.
- 806 Truman, R.W., and Krahenbuhl, J.L. (2001). Viable *M. leprae* as a research reagent. *Int J Lepr*
807 *Other Mycobact Dis* *69*, 1-12.
- 808 Urbonavicius, J., Qian, Q., Durand, J.M., Hagervall, T.G., and Bjork, G.R. (2001).
809 Improvement of reading frame maintenance is a common function for several tRNA
810 modifications. *The EMBO journal* *20*, 4863-4873.
- 811 Vonrhein, C., Flensburg, C., Keller, P., Sharff, A., Smart, O., Paciorek, W., Womack, T., and
812 Bricogne, G. (2011). Data processing and analysis with the autoPROC toolbox. *Acta*
813 *crystallographica Section D, Biological crystallography* *67*, 293-302.
- 814 Whitehouse, A.J., Thomas, S.E., Brown, K., Fanourakis, A., Chan, D.S.H., Libardo, M.D.J.,
815 Mendes, V., Boshoff, H.I.M., Floto, R.A., Abell, C., *et al.* (2019). Development of inhibitors
816 against *Mycobacterium abscessus* tRNA (m¹G37) methyltransferase (TrmD) using fragment-
817 based approaches. ChemRxiv. Preprint. <https://doi.org/10.26434/chemrxiv.8131847.v1>.

818 Winn, M.D., Ballard, C.C., Cowtan, K.D., Dodson, E.J., Emsley, P., Evans, P.R., Keegan, R.M.,
819 Krissinel, E.B., Leslie, A.G., McCoy, A., *et al.* (2011). Overview of the CCP4 suite and current
820 developments. *Acta crystallographica Section D, Biological crystallography* 67, 235-242.

821 Zhang, Y., Agrebi, R., Bellows, L.E., Collet, J.F., Kaefer, V., and Grundling, A. (2017).
822 Evolutionary Adaptation of the Essential tRNA Methyltransferase TrmD to the Signaling
823 Molecule 3',5'-cAMP in Bacteria. *The Journal of biological chemistry* 292, 313-327.

824 Zhong, W., Koay, A., Ngo, A., Li, Y., Nah, Q., Wong, Y.H., Chionh, Y.H., Ng, H.Q., Koh-
825 Stenta, X., Poulsen, A., *et al.* (2019). Targeting the Bacterial Epitranscriptome for Antibiotic
826 Development: Discovery of Novel tRNA-(N(1)G37) Methyltransferase (TrmD) Inhibitors.
827 *ACS infectious diseases*.

828
829

830 **Author Contributions**

831 RAF, TLB, VM, AGC and CA conceived and managed the project. SET, AJW and VM wrote
832 the manuscript and designed the experiments. SET and PG performed the molecular biology
833 and expression, protein purification, characterization, crystallography and fragment library
834 screening. AJW designed, synthesized and characterised the compounds. SET and AJW
835 performed the biophysical and biochemical assays. KPB performed the microbiological
836 experiments on *M. abscessus*, *M. tuberculosis Bluepan* and NTMs. MDJL and HIMB
837 performed the microbiological experiments on *M. tuberculosis* H37Rv. MJ and JMB designed
838 and carried out the *trmD* knockout studies. RL designed and performed the experiments on *M.*
839 *leprae*. SM performed the bioinformatics studies and t-RNA sequence searches.

840

841 **Acknowledgements**

842 This work is funded by the Cystic Fibrosis Trust (Registered as a charity in England and Wales
843 (1079049) and in Scotland (SC040196)) Strategic research consortium and in part by the
844 Intramural Research Program of the NIH, NIAID. The authors would like to thank the Diamond
845 Light Source for beam-time (proposals mx9537, mx14043, mx18548) and the staff of
846 beamlines I03, I02, I04, I04-1 and I24 for assistance with data collection, the Seattle Structural
847 Genomics Consortium for kindly providing the *M. abscessus trmD* AVA0421 plasmid, Prof.

848 Ben Luisi and Dr. Kasia J. Bandrya (Department of Biochemistry, University of Cambridge)
849 for insights on experimental design using tRNA, Prof. Angelika Gründling (MRC Centre for
850 Molecular Bacteriology and Infection, Imperial College London) for kindly providing an *E.*
851 *coli* strain for the expression of *M. tuberculosis* TrmD, Dr. Sundeep Chaitanya (Department of
852 Biochemistry, University of Cambridge) for discussions on *M. leprae* inhibition studies. SET
853 is funded by the Cystic Fibrosis Trust (RG 70975) and Foundation Botnar (RG91317); VM is
854 funded by the Bill and Melinda Gates Foundation SHORTEN-TB (RG 86546); TLB is funded
855 by the Wellcome Trust (Wellcome Trust Investigator Award 200814_Z_16_Z: RG83114);
856 AJW is funded through the EPSRC. RAF, TLB and CA would like to thank the Foundation
857 Botnar for funding (Grant No. RG91317).

858

859 **Accession Numbers**

860 Coordinates and structure factors related to this work been deposited in the PDB with accession
861 numbers 6NVR, 6NW6, 6NW7, 6QO2, 6QO3,6QO4, 6QO6, 6QOA, 6QOC, 6QOD, 6QOE,
862 6QOF, 6QOG, 6QOH, 6QOI, 6QOJ, 6QOK, 6QOL, 6QOM, 6QON, 6QOO, 6QOP, 6QOQ,
863 6QOR, 6QOS, 6QOT, 6QOU, 6QOV, 6QOW, 6QOX, 6QQS, 6QQX, 6QQY, 6QR6, 6QR5
864 and 6QR8.

865

Figure 1

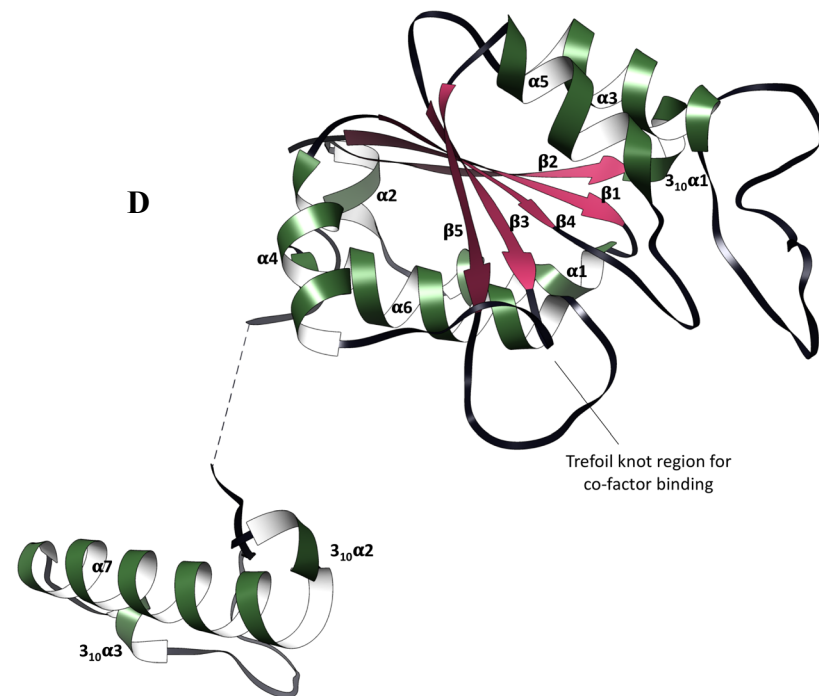
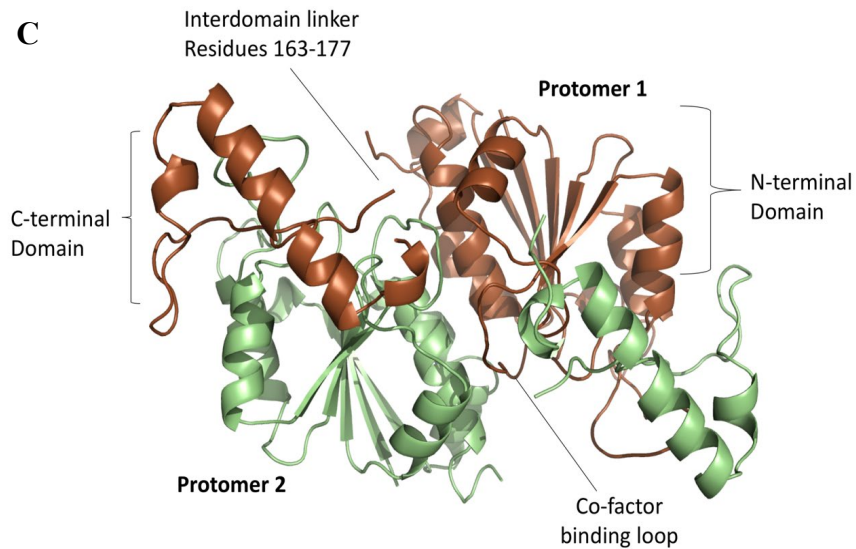
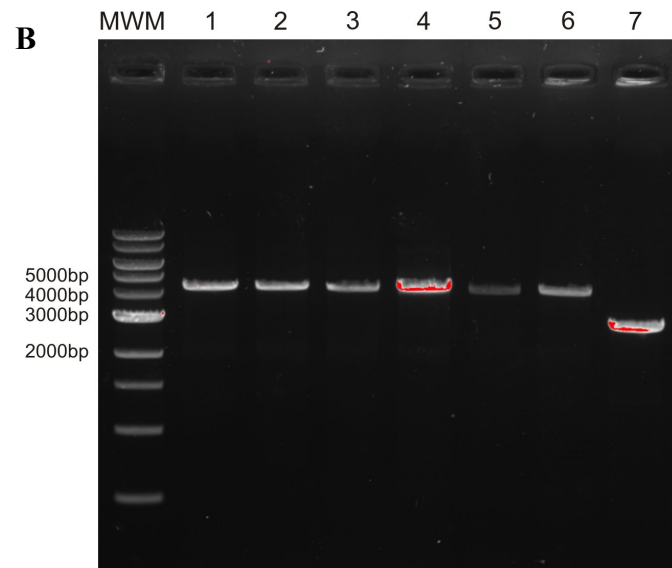
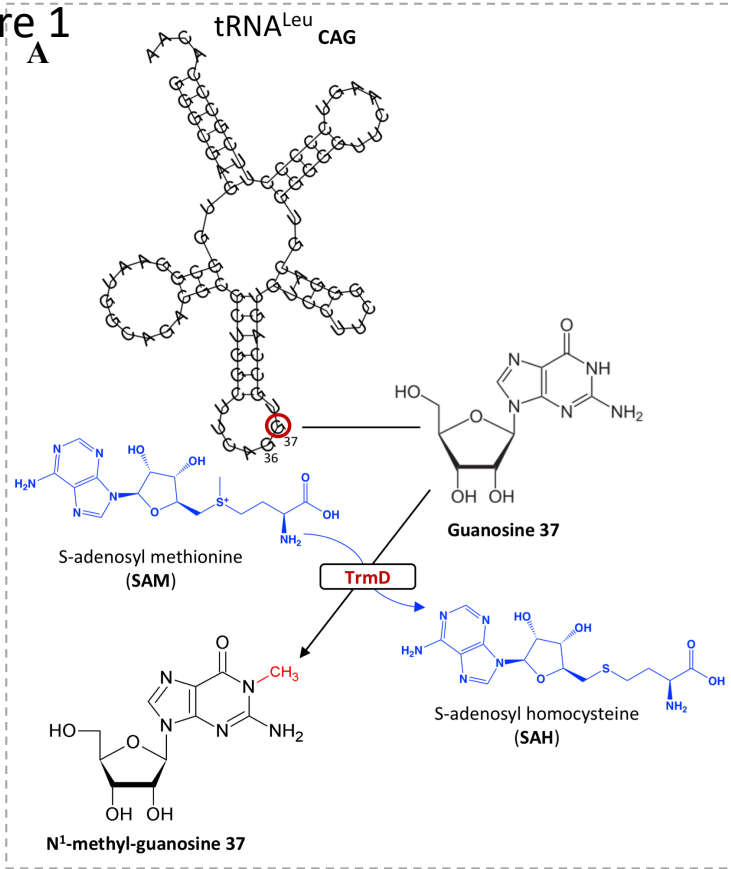


Figure 2

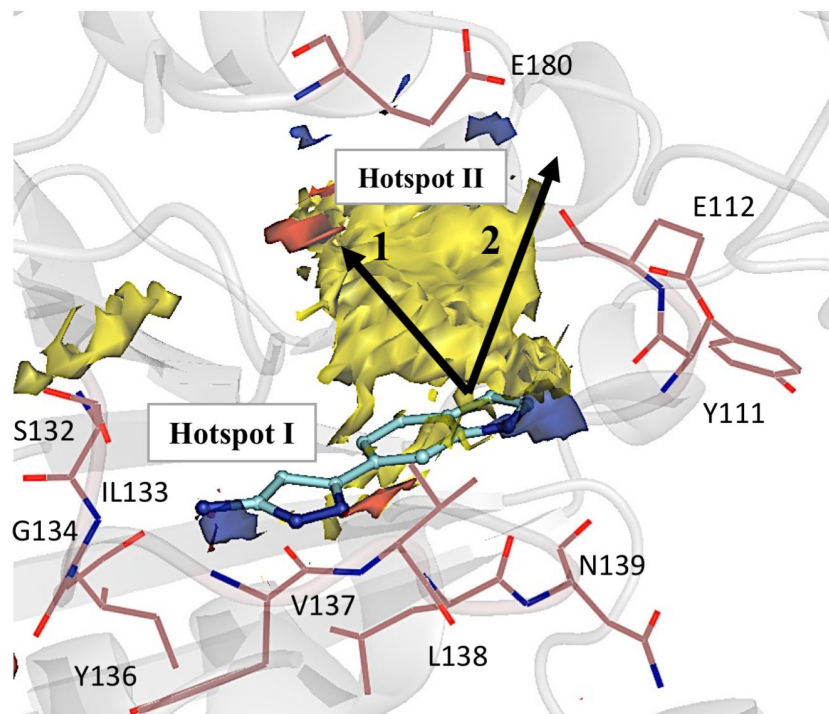
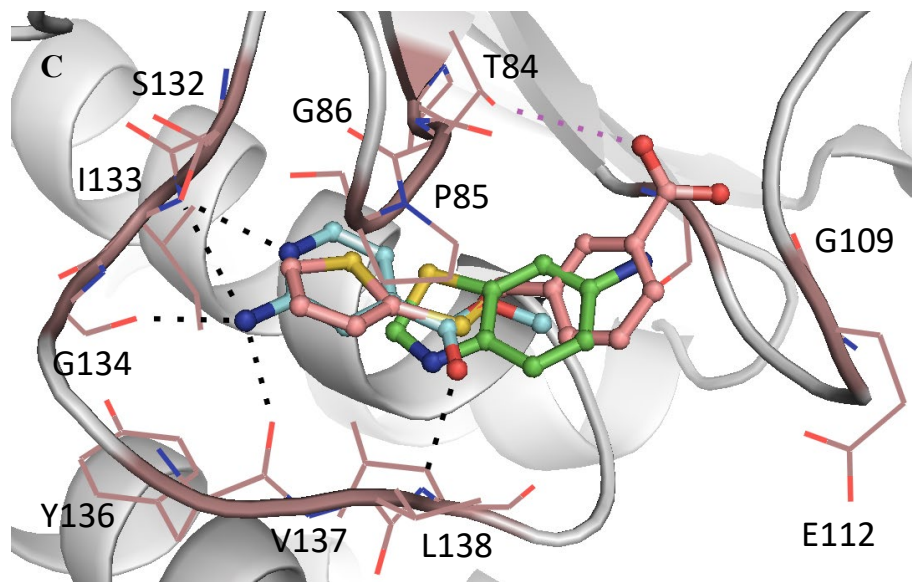
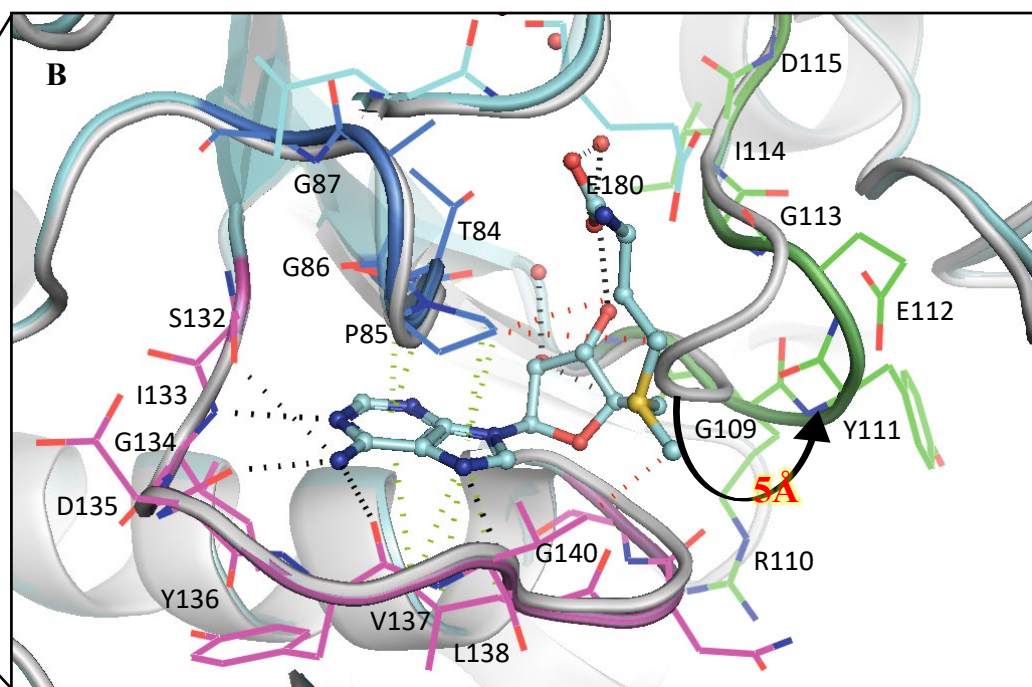
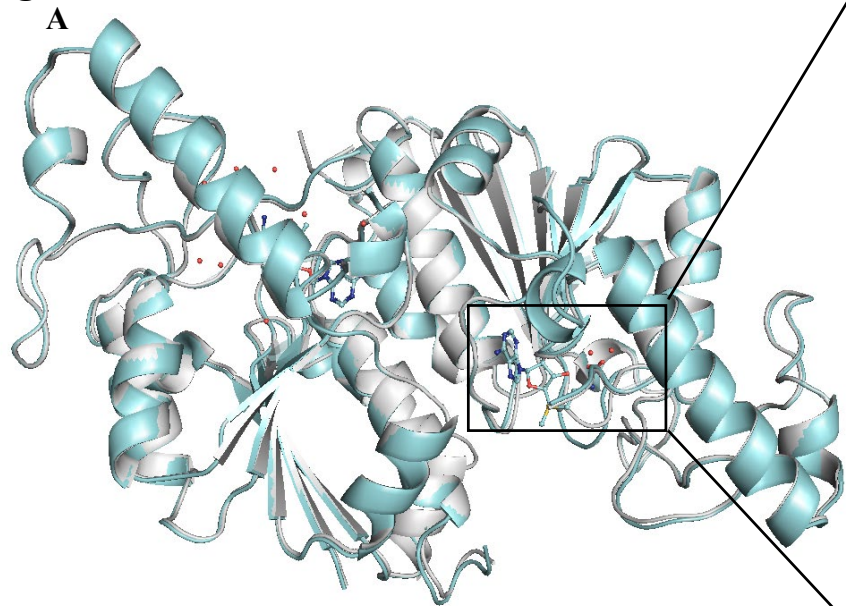


Figure 3

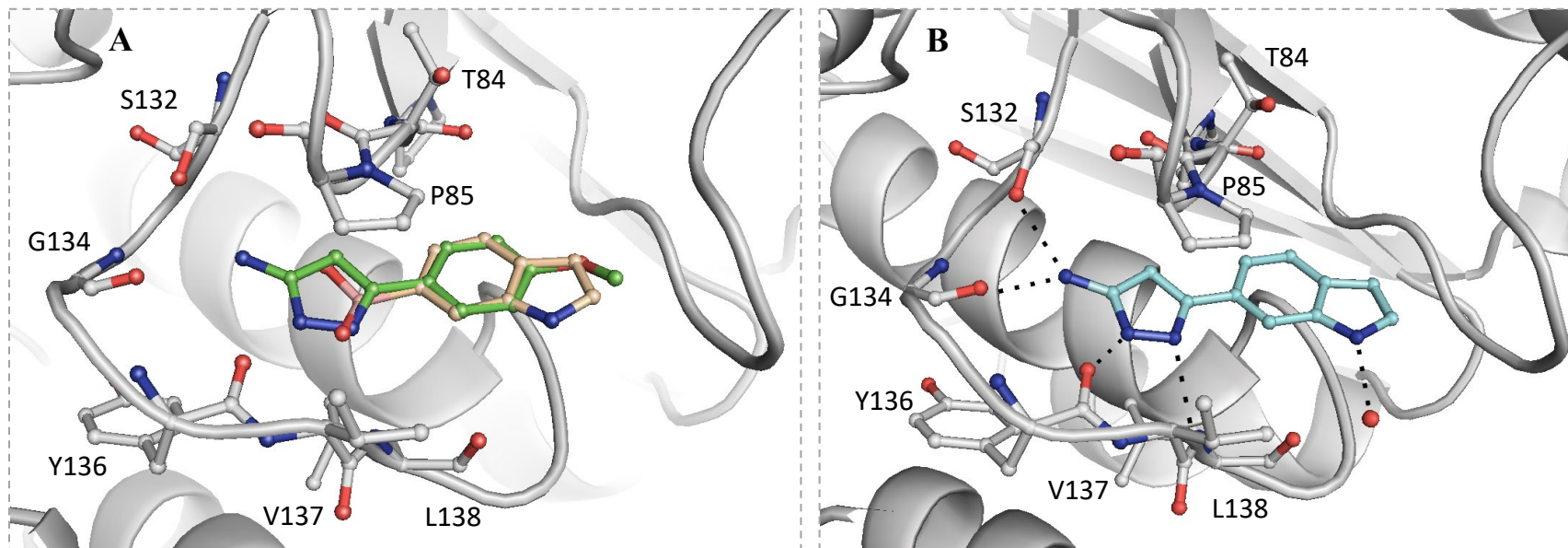


Figure 4

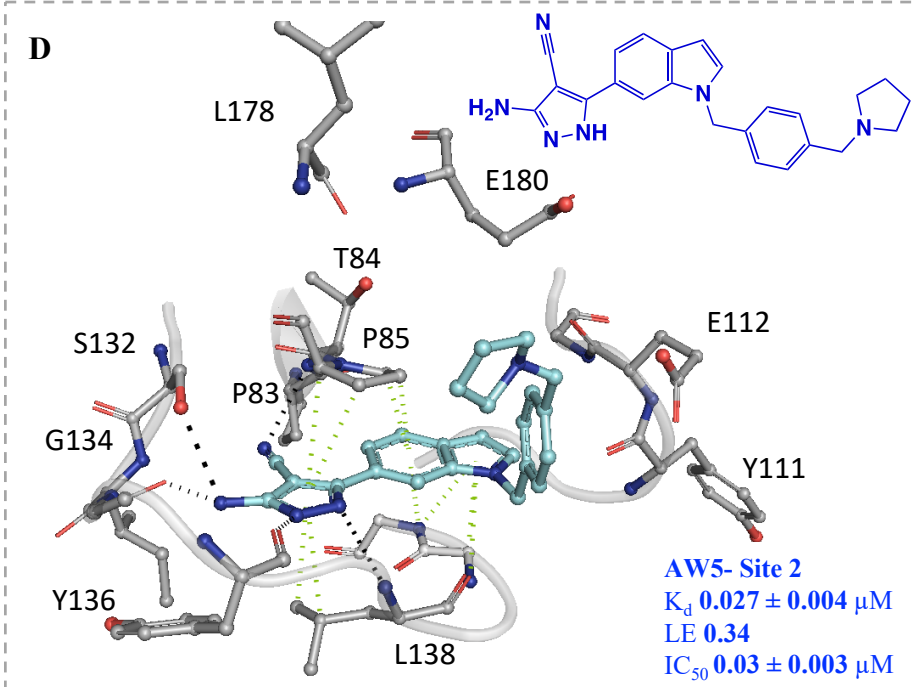
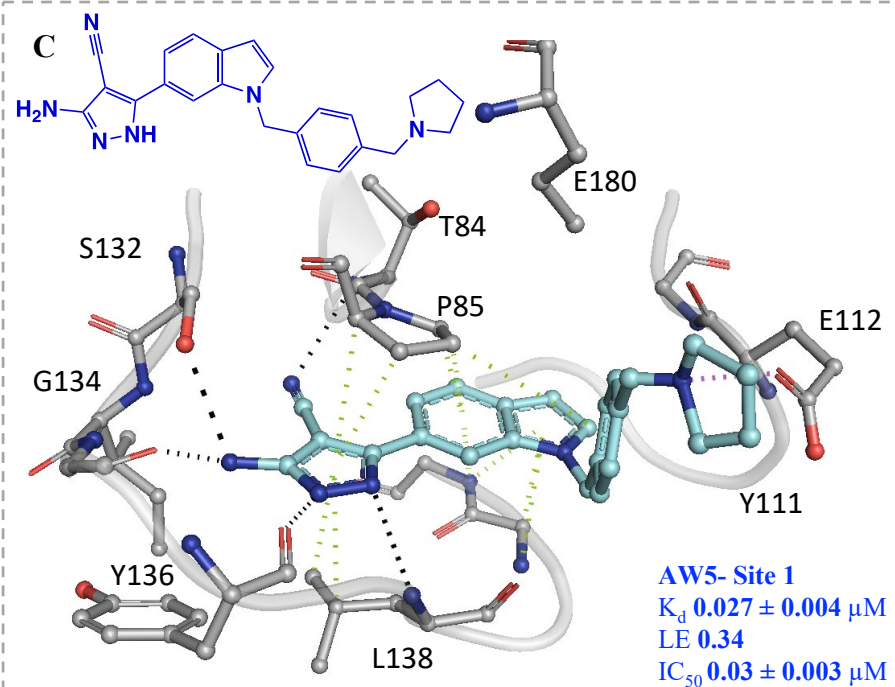
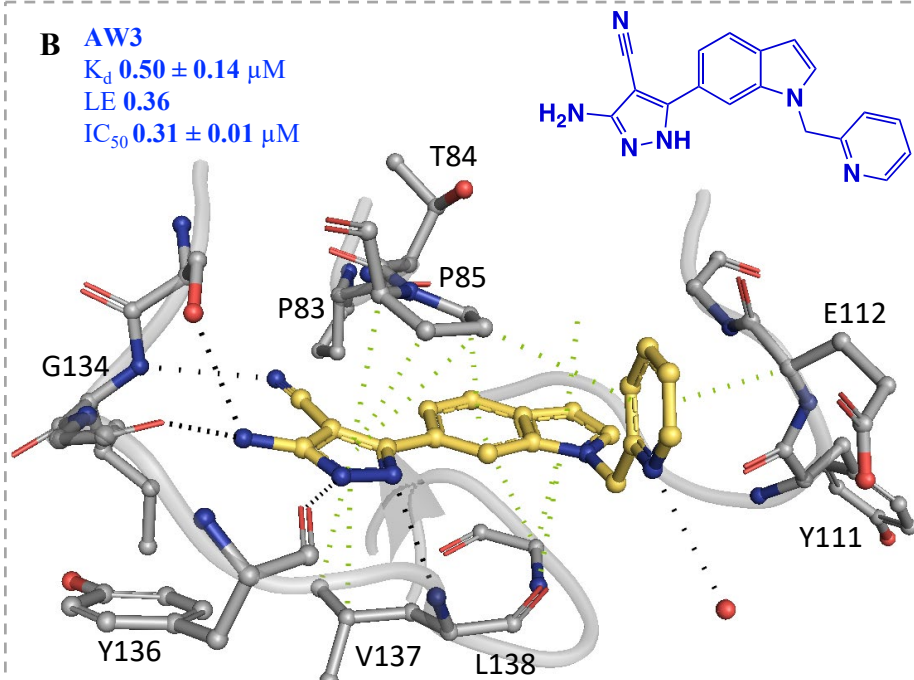
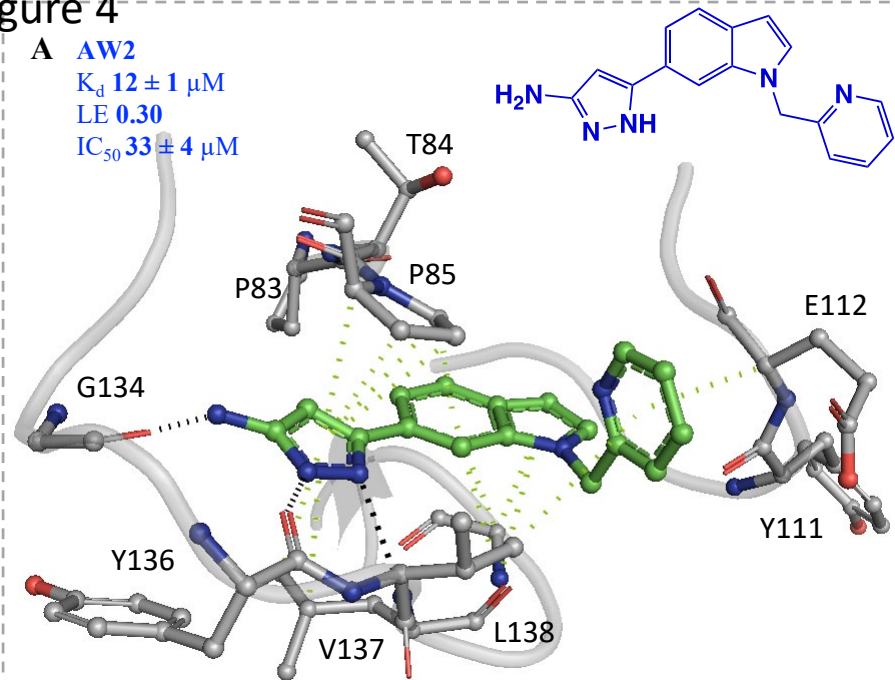
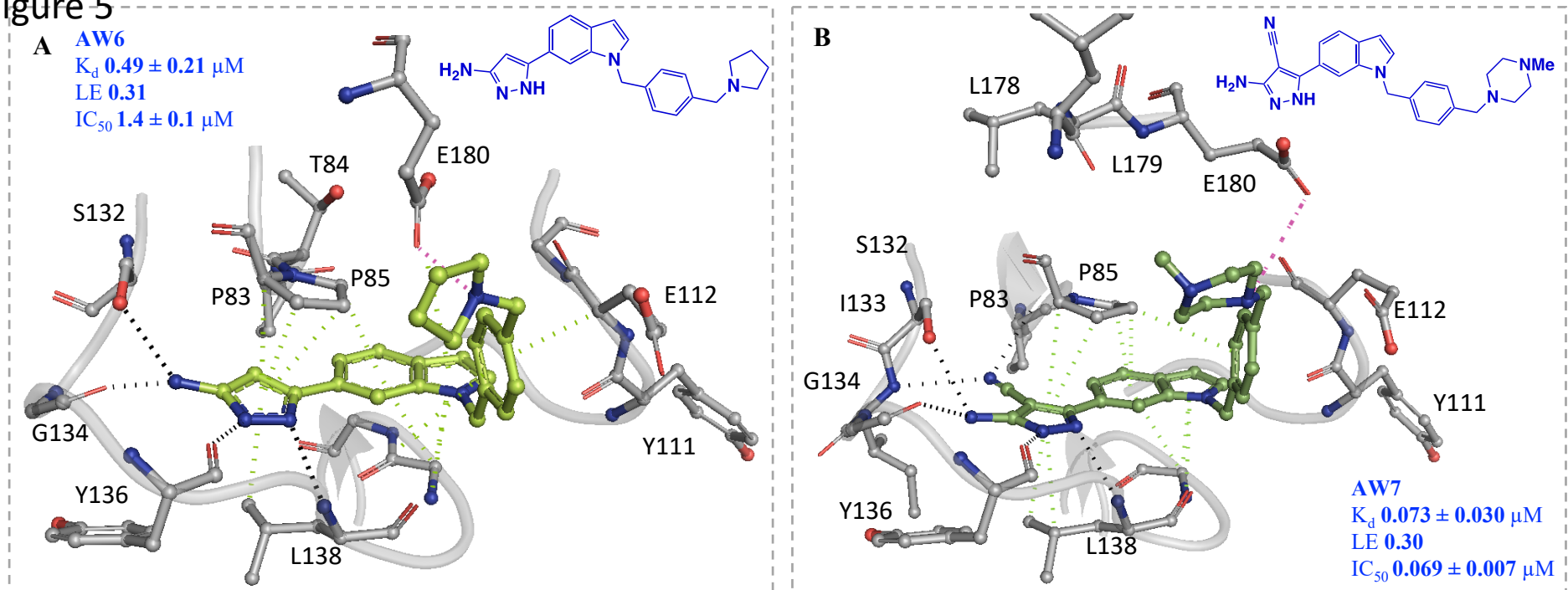
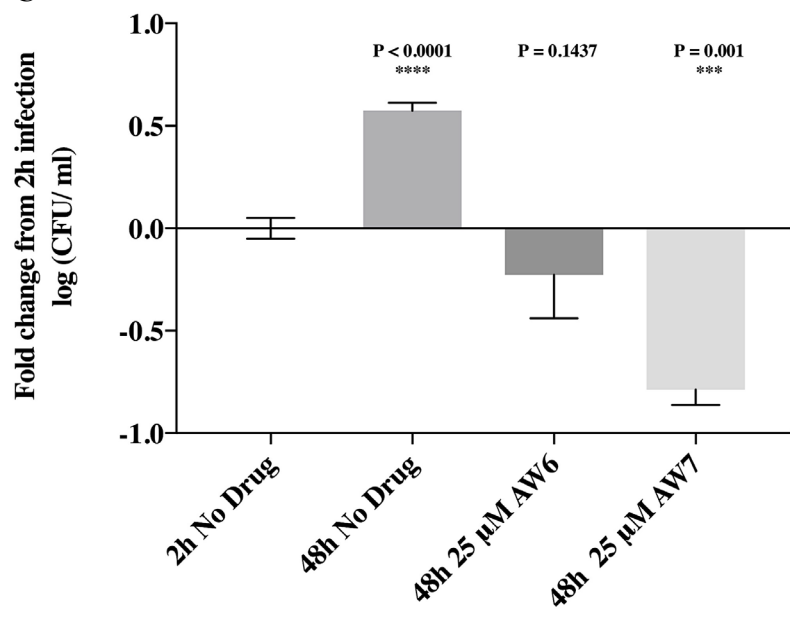


Figure 5**C** **Growth inhibition of *M. abscessus* in human macrophages****D** **% inhibition of β -oxidation rate of intracellular *M. leprae* in the presence of AW7**